Geoscience Frontiers 10 (2019) 315–330

HOSTED BY

Contents lists available at ScienceDirect

China University of Geosciences (Beijing)

Geoscience Frontiers

journal homepage: www.elsevier.com/locate/gsf

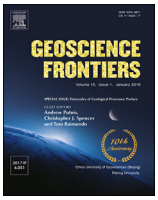

Research Paper

Cambro-Silurian magmatisms at the northern Gondwana margin (Penninic basement of the Ligurian Alps)

Matteo Maino [a,*], Laura Gaggero [b], Antonio Langone [c], Silvio Seno [a], Mark Fanning [d]

[a] Department of Earth and Environmental Sciences, University of Pavia, Via Ferrata 1, 27100 Pavia, Italy
[b] Department of Earth, Environment and Life Sciences, University of Genoa, Corso Europa 26, I-16132 Genoa, Italy
[c] CNR—Institute of Geosciences and Earth Resources, U.O.S. Pavia, Via Ferrata 1, 27100 Pavia, Italy
[d] Research School of Earth Sciences, The Australian National University, Canberra, ACT 0200, Australia

ARTICLE INFO

Article history:
Received 24 July 2017
Received in revised form
1 December 2017
Accepted 10 January 2018
Available online 27 February 2018
Handling Editor: Christopher J. Spencer

Keywords:
U–Pb zircon dating
Early Paleozoic magmatism
Pre-Alpine basements
Gondwana margin
Ligurian Alps

ABSTRACT

The Early Paleozoic evolution of the northern margin of Gondwana is characterized by several episodes of bimodal magmatism intruded or outpoured within thick sedimentary basins. These processes are well recorded in the Variscan blocks incorporated in the Ligurian Alps because they experienced low temperature Alpine metamorphism. During the Paleozoic, these blocks, together with the other Alpine basements, were placed between the Corsica-Sardinia and the Bohemian Massif along the northern margin of Gondwana. In this framework, they host several a variegated lithostratigraphy forming two main complexes (Complexs I and II) that can be distinguished by both the protoliths and their cross-cutting relationships, which indicate that the acidic and mafic intrusives of Complex II cut an already folded sequence made of sediments, basalts and granitoids of Complex I. Both complexes were involved in the Variscan orogenic phases as highlighted by the pervasive eclogite-amphibolite facies schistosity (foliation II). However, rare relicts of a metamorphic foliation at amphibolite facies conditions (foliation I) is locally preserved only in the rocks of Complex I. It is debatable if this schistosity was produced during the early folding event – occurred between the emplacement of Complex I and II – rather than during an early stage of the Variscan metamorphic cycle.

New SHRIMP and LA ICP-MS U–Pb zircon dating integrated with literature data, provide emplacement ages of the several volcanic or intrusive bodies of both complexes. The igneous activity of Complex I is dated between 507 ± 15 Ma and 494 ± 5 Ma, while Complex II between 467 ± 12 Ma and 445.5 ± 12 Ma. The folding event recorded only by the Complex I should therefore have occurred between 494 ± 5 Ma and 467 ± 12 Ma. The Variscan eclogite-amphibolite facies metamorphism is instead constrained between ~420 Ma and ~300 Ma. These ages and the geochemical signature of these rocks allow constraining the Early Paleozoic tectono-magmatic evolution of the Ligurian blocks, from a middle–upper Cambrian rifting stage, through the formation of an Early Ordovician volcanic arc during the Rheic Ocean subduction, until a Late Ordovician extension related to the arc collapse and subsequent rifting of the PaleoThetys. Furthermore, the ~420–350 Ma ages from zircon rims testify to thermal perturbations that may be associated with the Silurian rifting-related magmatism, followed by the subduction-collisional phases of the Variscan orogeny.

1. Introduction

The basement of the European Alps preserves relicts of the pre-Variscan geological history of domains that belonged to the northern Gondwana margin (Ziegler, 1984; von Raumer, 1998; von Raumer et al., 2003; Nance et al., 2010; Stampfli et al., 2011; Franke et al., 2017). The External Crystalline Massifs of the Alps (e.g. Aar-Gotthard, Aiguilles-Rouges-Mont-Blanc, Pelvoux-Belledonne, Argentera) experienced low-grade metamorphism during the Alpine cycle and thus preserve the best record of the pre-Variscan and Variscan magmatic and metamorphic evolution (e.g. Bussy and von Raumer, 1994; von Raumer, 1998; Bussy et al., 2000; Guillot

* Corresponding author.
E-mail address: matteo.maino@unipv.it (M. Maino).
Peer-review under responsibility of China University of Geosciences (Beijing).

https://doi.org/10.1016/j.gsf.2018.01.003

et al., 2002; von Raumer et al., 2002, 2003, 2009; Schaltegger et al., 2003). Conversely, the internal zones of the Alps (i.e. the Penninic domain) were generally intensely overprinted by the Alpine tectono-metamorphic events and the Variscan blocks were dismembered into multiple nappes, making it difficult to recognize the primary relationships. In this case, isotopic dating and geochemistry of igneous rocks of the Paleozoic relicts are the only available tools to provide constraints in the reconstruction of the pre-Alpine evolution.

The Lower Paleozoic evolution of the Alpine basements is characterized by the record of two successive subduction cycles, which are classically referred to as the Cambrian–Ordovician and the Devonian–Carboniferous – or Variscan cycle (e.g. Guillot et al., 1991; Bussy and von Raumer, 1994; Bussy et al., 1996; Schaltegger and Gebauer, 1999; Bertrand et al., 2000; Guillot et al., 2002; von Raumer et al., 2002, 2003, 2013; Schaltegger et al., 2003; von Raumer and Stampfli, 2008). During the Cambrian–Ordovician cycle, the northern margin of Gondwana experienced multiple phases of rifting and subduction, followed by Late Ordovician–Silurian crustal extension likely associated with the opening of Palaeotethys (or South Armorica Ocean; e.g. Linnemann et al., 2007, 2008; von Raumer and Stampfli, 2008; Rossi et al., 2009; Nance et al., 2010; Gaggero et al., 2012). The Cambro–Ordovician geodynamic phases were characterized by the emplacement of huge volumes of both acidic and mafic igneous bodies between ~530 Ma and ~450 Ma (e.g. Bussy and von Raumer, 1994; Bertrand et al., 2000; von Raumer et al., 2002; Schaltegger et al., 2003; Oggiano et al., 2010; Gaggero et al., 2012). During the Late Ordovician–Silurian, the igneous activity in the basements of the Alpine domain tends to disappear, although some evidences of thermal events producing local crustal melting are recorded in the External, Austroalpine and Carnic domains (Paquette et al., 1989; Schaltegger, 1993; Thony et al., 2008; Schulz and von Raumer, 2011). Since the Devonian, the Rheic Ocean subduction and the opening of the Palaeotethys at the Gondwana margin mark the starting of the Variscan cycle, which deeply modified the Alpine basements through multiple tectono-metamorphic and magmatic phases (e.g. Matte, 1986, 2001; von Raumer et al., 2003, 2013).

Although this general evolution is well recorded in the Alpine basements that escaped the Cenozoic high-grade metamorphism (i.e. the External Massifs), the internal zones of the Alps (the Penninic domain) lack a complete geochronological dataset constraining all the distinct geodynamic steps. New findings from Penninic basements are therefore needed to better characterize their pre-Variscan history in comparison with the other basements derived from the northern Gondwana margin.

The present study focuses on the dating of Early Paleozoic magmatic rocks from Variscan blocks dismembered into several Penninic nappes of the southernmost branch of the Alpine chain – i.e. the Ligurian Alps (Fig. 1). During the Paleozoic, the Ligurian Alps represented the connection between the Bohemian and Alpine basements toward East and the Sardinia-Corse-Maures massifs toward West, thus representing a key sector of the Southern Variscides (Cortesogno et al., 2004; Dallagiovanna et al., 2009; Rossi et al., 2009; Casini et al., 2012, 2015a,b). We investigated intrusive and volcanic rocks until now attributed to the Cambrian–Ordovician cycle on the basis of regional comparisons and few isotope dilution TIMS U–Pb zircon data (Cortesogno et al., 1993; Molina, 2002; Gaggero et al., 2004). The magmatic products were emplaced at different positions within the pre-Variscan crustal section: the metagranitoids intruded within relatively deep (high-T amphibolite facies) or middle (greenschist-lower amphibolite facies) crust, while the volcanites outpoured within sediments. The new geochronological data allow defining the timing of the magmatic episodes and thus constraining the Early Paleozoic evolution of the Ligurian basements within the frame of the northern Gondwana margin. Furthermore, our study documents for the first time the occurrence in the Penninic domain of a Late Ordovician–Silurian thermal event associated with thermal perturbations marking the transition between the Cambro–Ordovician and the Variscan cycles.

2. Geological setting

The Ligurian Alps preserve several pre-Alpine basements dismembered between the Penninic realm of the Western Alps (Fig. 1; e.g. Vanossi et al., 1986; Cortesogno et al., 1993; Seno et al., 2005; Maino et al., 2012b; Decarlis et al., 2013, 2014). The Penninic realm is constituted by three domains – Piedmont-Ligurian, Prepiedmont and Briançonnais – representing the Mesozoic ocean crust and the internal and external distal margins of the European crust, respectively (Decarlis et al., 2013, 2017). The External Crystalline Massifs of the Alps, instead, form the basement of the Dauphinois-Helvetic realm of the Alps, i.e. the proximal, relatively stable margin of Europe (Lemoine et al., 1986; Decarlis et al., 2013). Since the Cretaceous onward, in consequence of the convergence between the Adria (a promontory of the Africa plate) and European plates, the Piedmont-Ligurian Ocean was subducted beneath the Adria, leading the subsequent collision between the two plates (e.g. Vanossi et al., 1986; Schmid et al., 1996). During this Cenozoic tectono-metamorphic cycle, the Ligurian Paleozoic basements (hosted in both Briançonnais and Prepiedmont continental domains) experienced different metamorphic conditions, from eclogite (Torrente Visone unit), blueschist (Bagnaschino, Savona, Nucetto and Costa Dardella massifs) to greenschist facies (Arenzano, Calizzano, Pallare massifs) (Messiga et al., 1992; Cortesogno et al., 1993, 1997, 2002; Desmons et al., 1999b; Seno et al., 2005; Decarlis et al., 2017). However, the main temperature conditions attained by the basements during the post-Variscan phases did not exceed ~300–350 °C (Messiga et al., 1981; Maino et al., 2012a, 2015b; Decarlis et al., 2017), thus preserving an important record of the pre- and Variscan tectono-metamorphic features of the basements. In spite of the Alpine overprint, the pristine lithostratigraphic, metamorphic and tectonic complexity may be recognized after the deconvolution of the Alpine deformation (Cortesogno et al., 1993; Seno et al., 2005, 2010; Maino et al., 2012b, 2015a; Maino and Seno, 2016).

The complete sequence of the Ligurian pre-Variscan basement encompasses two main lithologic complexes (Fig. 2; Cortesogno, 1986; Cortesogno et al., 1993, 1997, 2004; Desmons et al., 1999a; Gaggero et al., 2004; Seno et al., 2010): (i) a gneiss-amphibolite complex (paragneisses I, metarhyolites I, orthogneisses and amphibolites I) locally enveloping small ultramafic bodies (Complex I); (ii) rocks of Complex I were folded and then intruded by large volumes of metagranitoids (orthogneisses II) or covered by minor remnants of a volcano-sedimentary sequence (paragneisses and metarhyolites II), locally including minor lenses of metagabbros, eclogites and migmatites (Complex II).

Both complexes are characterized by a main, pervasive schistosity (foliation II), which is associated with the Variscan structure and the related eclogite-amphibolite parageneses (Cortesogno, 1986; Vanossi et al., 1986; Cortesogno et al., 1993, 1997; Desmons et al., 1999b; Gaggero et al., 2004; Seno et al., 2010). Furthermore, rocks of Complex I locally preserve a few relicts of an older amphibolite-facies foliation (foliation I) that is partially or completely transposed along the foliation II (e.g. Cortesogno et al., 1993; Desmons et al., 1999a; Gaggero et al., 2004). However, it is not clearly proven with microstructural and petrographic investigations, if these relicts were developed during an early stage of

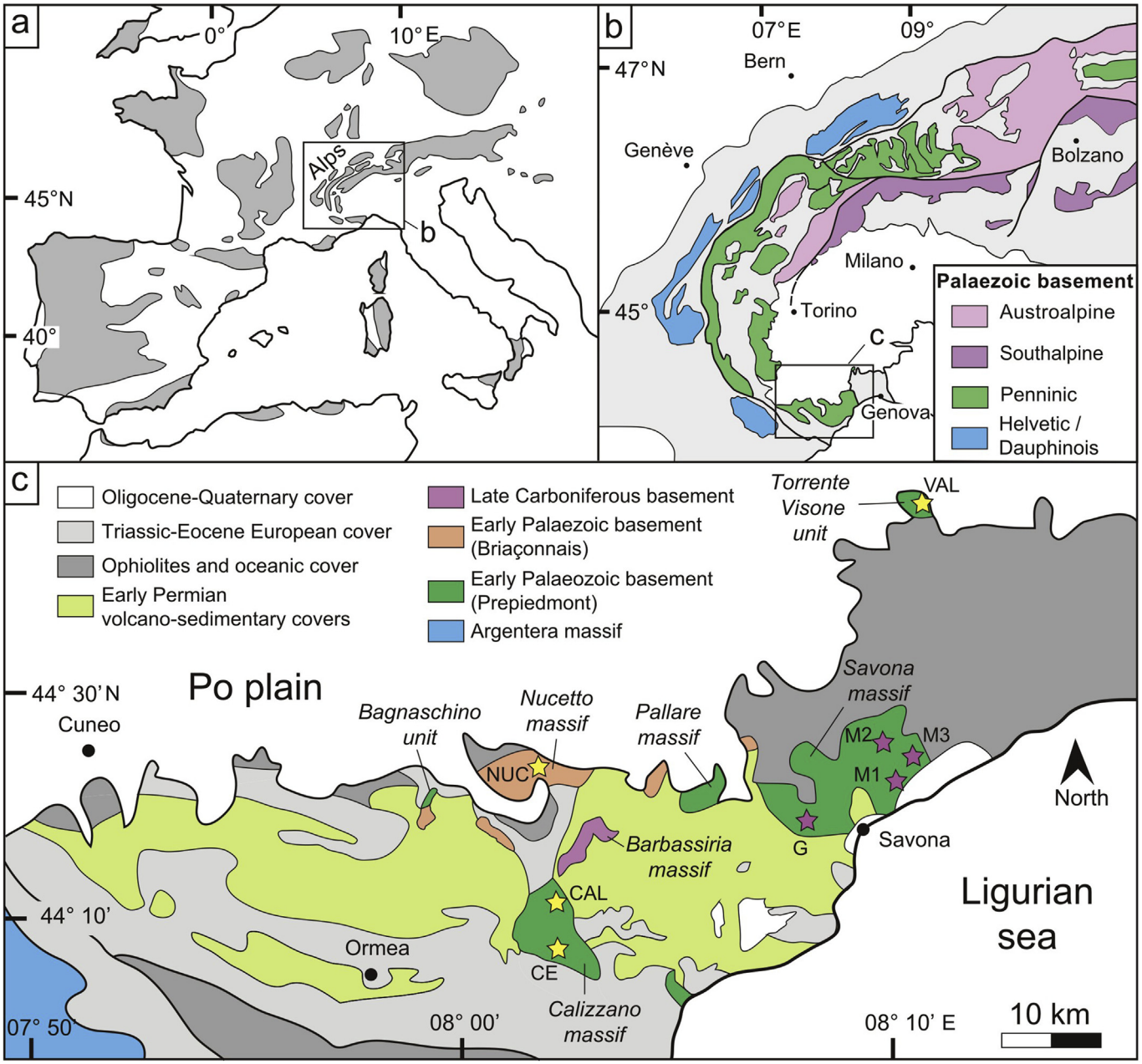

Figure 1. (a) Distribution of the main Variscan basements in Europe and (b) in the Western/Central Alps (modified after von Raumer et al., 2002). (c) Simplified geological map of the Ligurian Alps (from Maino et al., 2012b, 2013). Locations of sampling sites for U–Pb analyses are shown as yellow (this study) and violet stars (sample G from Giacomini et al., 2007; samples M1-3 from Molina, 2002).

the Variscan cycle rather than during a distinct pre-Variscan tectono-metamorphic event. In this case, this schistosity should have been generated during the folding predating the Complex II rocks. Until now, in absence of geochronological dating, literature data tend to attribute the foliation I to an early Paleozoic tectono-metamorphic phase, inasmuch as field relationships indicate that the younger intrusives of Complex II cut the previously folded sequence of paragneisses, orthogneisses and amphibolites of the Complex I (for further details see Cortesogno et al., 1993; Gaggero et al., 2004; Seno et al., 2010). The relationships between complexes I and II are observable only in the Prepiedmont Calizzano and Savona massifs, while the Briançonnais basements (i.e. the Nucetto massif) are constituted only by the younger orthogneisses and paragneisses of Complex II.

The small basement fragment of the Torrente Visone unit shows a peculiar lithostratigraphy, dismembered in two parts: a lower sub-unit of a volcano-sedimentary sequence (metarhyolites, paragneisses, micaschists and marbles) encompassing metabasic boudins and an upper sub-unit of detritic carbonate metasediments and metapelites embedding lenses of metabasites and serpentinites. Faint relicts of a pre-Alpine paragenesis within the orthogneisses (garnet, zoisite, biotite and muscovite) and metabasites (garnet) are interpreted to record the pre-Alpine metamorphic history (Cabella et al., 1990, 1991); however, in absence of a radiometric dating, an Alpine origin of this unit could not be excluded.

The ages of the magmatic protoliths of the Ligurian basements are poorly constrained. Published geochronological data from the

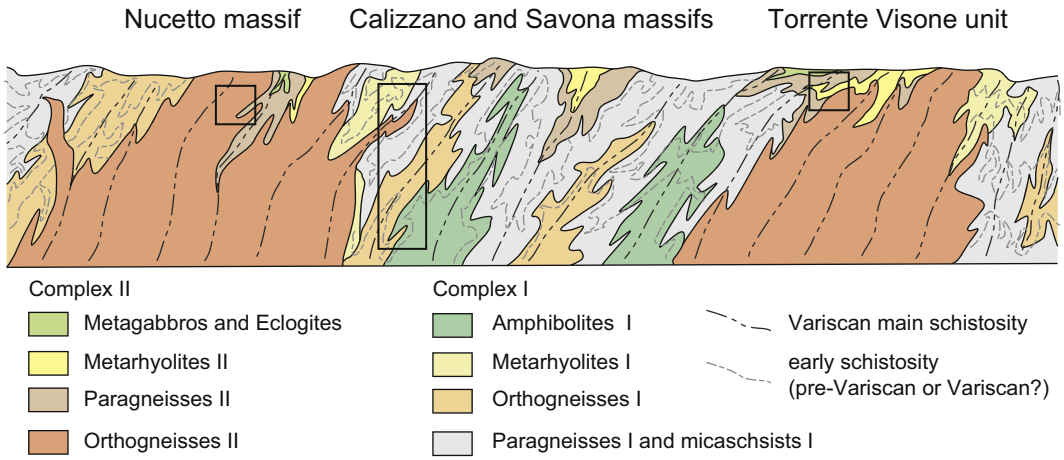

Figure 2. Idealized crustal section of the Ligurian sector at the end of the Variscan phase (Late Carboniferous) showing the relationships between the two main lithostratigraphic complexes (I and II) before the Alpine dismembering in several basement units.

Savona Massif constrain the age of the granites (now orthogneisses I) from the Complex I (ID TIMS U–Pb age of 494 ± 5 Ma) and the peraluminous monzogranites (now orthogneisses II) from the Complex II (two ID TIMS U–Pb ages of 473 ± 1 Ma and 468 ± 1 Ma; Molina, 2002) as well as the ~468 Ma age of the basaltic melts that were transformed into eclogites and amphibolitised gabbros of the Complex II (LA-ICP MS U–Pb data; Giacomini et al., 2007; Cruciani et al., 2015).

The parageneses developed on the foliation I (garnet-kyanite-sillimanite-staurolite in the paragneisses, garnet-diopside-green hornblende-plagioclase in the amphibolites) indicate amphibolite facies conditions (P of 0.6–0.8 GPa and T ~650 °C; Messiga et al., 1992; Cortesogno et al., 1993, 1997; Gaggero et al., 2004); there are not geochronological data constraining this metamorphic stage. The main schistosity (foliation II) involving both complexes I and II is, instead, better constrained: an Eo-Variscan metamorphic peak reached by the small bodies of migmatites and eclogites of complex II ($P \geq$ 1.7 GPa and T ~760 °C; Cortesogno, 1986; Cortesogno et al., 1993, 1997, 2004; Desmons et al., 1999a; Gaggero et al., 2004) is dated between 420 Ma and 400 Ma (zircon U–Pb data; Giacomini et al., 2007), while the regional amphibolite facies metamorphism (P ~0.4 GPa and T ~600 °C) and the following greenschist facies retrogression (Messiga et al., 1992; Cortesogno et al., 1993, 1997; Desmons et al., 1999a; Gaggero et al., 2004) are constrained by several U–Pb, Rb/Sr and Ar/Ar data between ~392 Ma and ~300 Ma (Del Moro et al., 1981; Barbieri et al., 2003; Giacomini et al., 2007). The late- to post-Variscan evolution is characterized by orogen exhumation and wrenching tectonics accompanied by the emplacement of huge volumes of volcanites and minor intrusive bodies between ~315 Ma and ~260 Ma (Dallagiovanna et al., 2009; Maino et al., 2012b).

3. Methods

This study addresses the petrographic and geochronological features of one sample of metarhyolite from the Complex I (Calizzano massif), two orthogneisses and one metarhyolite from the Complex II (Calizzano, Nucetto and Torrente Visone massifs). Samples were chosen in order to be representative of the largest outcrops characterizing the main igneous (intrusive and effusive) bodies of the two complexes. Sample localities have been selected far from Alpine or Variscan shear zones that can deeply modify the thermal record of deformed rocks (Maino et al., 2015b).

3.1. Geochronology

Zircon grains for geochronological investigations were separated using standard procedure of grinding, sieving, magnetic and density separation. Intact or low damage grains under a binocular microscope were hand-picked, mounted in epoxy resin and polished with 0.25 μm diamond paste. Zircon structures were investigated with backscattered electron (BSE) microscopy and cathodoluminescence (CL) by a scanning electron microscope (SEM-JEOL JXA840) at CNR-IGG-Pavia. Locations of the spot-analysis were selected from the CL images in order to avoid damaged or altered zones, and, possibly, to prevent analyses of areas where different structural domain overlap.

U–Pb geochronology was carried out with two different instruments: a SHRIMP-II at the Australian National University, Canberra, and an excimer laser ablation (LA) ICP-MS at the CNR-IGG-Pavia. The SHRIMP analyses followed the analytical procedure of Williams (1998) and Elliot et al. (2016). Each analysis consisted of 4 scans through the mass range, with Duluth gabbro standard (1099.1 ± 0.5 Ma; Paces and Miller, 1993). Error in the standard calibration was lower than 0.5% for the analytical sessions (Table 1; Supplementary Table 1). The spot size was set to 20 μm. Correction for common Pb was made using the measured $^{204}Pb/^{206}Pb$ and $^{207}Pb/^{206}Pb$ ratios following Tera and Wasserburg (1972) as outlined in Williams (1998). Data reduction was performed using the SQUID Excel Macro of Ludwig (2001).

The second instrument consists of a 193 nm ArF excimer laser ablation system (Geolas200Q-Microlas) and a high-resolution sector field ICP-MS (Element I from ThermoFinnigan), following the analytical method of Tiepolo (2003) and Gaggero et al. (2017). The spot size of the instrument was mostly set to 20 μm, apart a few analyses that have been performed at 10 μm (Supplementary Table 2). The U–Pb ratio was calibrated with the 91500-zircon standard (1065 Ma, Wiedenbeck et al., 1995); the relative standard deviation of the analyses was lower than 2% for analyses acquired with a spot size of 20 μm spot, while up to 3.9% for the few analyses acquired at 10 μm (Table 2; Supplementary Table 2). The reproducibility of the standards was numerically propagated through all age determinations according to the equation of Horstwood et al. (2003). The zircon standard 02123 (295 Ma; Ketchum et al., 2001) was analyzed in parallel with the unknown samples for quality control. In this case, the presence of common Pb was evaluated in each analysis on the basis of the net signal of ^{204}Pb (i.e., subtracted

Table 1
Summary of SHRIMP II isotope analyses and calculated $^{206}Pb/^{238}U$ ages for the metarhyolite of Complex I (sample CE) and orthogneisses from Complex II (sample CAL) sampled in the Calizzano massif. c = core, o = oscillatory zoned overgrowths, r = rim or homogeneous patches, f = fractured or damaged grain. See Supplementary Table 1 for the complete dataset.

Sample CE															
Lat 44°11′11″N															
Long 8°7′46″E															
Grain spot	Spot location	U (ppm)	Th (ppm)	Th/U	$^{206}Pb^{c}$ (ppm)	$^{204}Pb/^{206}Pb$	$f_{206}{}^{b}$ (%)	Total ratios						Age (Ma)	
								$^{238}U/^{206}Pb$	error[a] ±	$^{207}Pb/^{206}Pb$	error[a] ±	$^{206}Pb/^{238}U$	error[a] ±	$^{206}Pb/^{238}U$	error[a] ±
1.1	o (f)	71	44	0.62	4.7	0.000848	2.26	12.988	0.200	0.0747	0.0033	0.0753	0.0012	467.7	7.4
2.1	o	133	38	0.29	9.4	0.000000	0.29	12.135	0.146	0.0598	0.0014	0.0822	0.0010	509.0	6.0
3.1	o	112	91	0.81	7.9	0.000214	0.15	12.273	0.156	0.0585	0.0012	0.0814	0.0011	504.2	6.3
4.1	o	117	1	0.01	8.1	0.000478	0.13	12.367	0.153	0.0583	0.0013	0.0808	0.0010	500.6	6.1
4.2	c	311	61	0.20	35.2	0.000079	1.12	7.607	0.071	0.0747	0.0006	0.1300	0.0013	787.8	7.2
5.1	o	598	238	0.40	42.1	0.000055	0.06	12.196	0.106	0.0579	0.0005	0.0819	0.0007	507.7	4.3
6.1	o (f)	88	18	0.21	5.9	0.000776	1.01	12.691	0.173	0.0650	0.0015	0.0780	0.0011	484.2	6.6
7.1	o (f)	53	5	0.09	4.1	0.016648	29.84	10.910	0.177	0.2961	0.0126	0.0643	0.0039	401.7	23.4
7.2	o	88	73	0.82	6.3	0.000452	<0.01	12.035	0.170	0.0570	0.0014	0.0832	0.0012	514.9	7.1
8.1	o	376	105	0.28	26.6	0.000062	0.06	12.137	0.115	0.0580	0.0010	0.0823	0.0008	510.1	4.8
8.2	c	96	59	0.62	16.8	0.000148	0.27	4.912	0.062	0.0821	0.0012	0.2030	0.0027	1192	15
9.1	o	126	47	0.37	8.7	0.000461	0.63	12.396	0.157	0.0622	0.0012	0.0802	0.0010	497.1	6.2
9.2	c	348	86	0.25	29.6	0.000488	0.57	10.110	0.105	0.0647	0.0006	0.0983	0.0011	604.7	6.2
10.1	o/c	198	101	0.51	14.4	0.000253	0.10	11.788	0.118	0.0586	0.0008	0.0847	0.0009	524.4	5.2
11.1	c	18	1	0.04	4.2	0.000387	11.98	3.589	0.114	0.1919	0.0081	0.2453	0.0098	1414	50
12.1	o	74	55	0.74	5.1	0.000224	0.43	12.384	0.167	0.0607	0.0015	0.0804	0.0011	498.5	6.7
13.1	o	117	61	0.52	8.4	0.000343	0.17	11.913	0.139	0.0591	0.0011	0.0838	0.0010	518.8	6.0
13.2	o	67	17	0.25	4.7	0.000301	0.24	12.288	0.169	0.0592	0.0015	0.0812	0.0011	503.2	6.8
Sample CAL															
Lat 44°13′16″N															
Long 8°5′17″E															
Grain spot	Spot location	U (ppm)	Th (ppm)	Th/U	$^{206}Pb^{c}$ (ppm)	$^{204}Pb/^{206}Pb$	$f_{206}{}^{b}$ (%)	Total Ratios						Age (Ma)	
								$^{238}U/^{206}Pb$	error[a] ±	$^{207}Pb/^{206}Pb$	error[a] ±	$^{206}Pb/^{238}U$	error[a] ±	$^{206}Pb/^{238}U$	error[a] ±
1.1	o	313	68	0.22	20.1	0.000173	0.25	13.352	0.138	0.0583	0.0008	0.0747	0.0008	464.5	4.7
2.1	o	435	56	0.13	27.6	0.000054	0.30	13.536	0.131	0.0586	0.0007	0.0737	0.0007	458.2	4.4
3.1	o	337	24	0.07	21.8	0.000263	0.16	13.259	0.135	0.0577	0.0008	0.0753	0.0008	468.0	4.7
4.1	o	265	64	0.24	17.1	0.000179	0.26	13.304	0.145	0.0584	0.0009	0.0750	0.0008	466.0	5.0
5.1	o	636	48	0.07	41.4	0.000033	0.13	13.221	0.120	0.0575	0.0006	0.0755	0.0007	469.5	4.2
6.1	c	141	62	0.44	14.2	–	0.06	8.550	0.105	0.0636	0.0011	0.1169	0.0015	712.7	8.5
6.2	c/o	485	76	0.16	32.2	0.000180	0.27	12.951	0.122	0.0589	0.0008	0.0770	0.0007	478.2	4.4
7.1	c	466	110	0.24	48.6	–	0.22	8.242	0.074	0.0657	0.0006	0.1211	0.0011	736.6	6.5
7.2	o	195	12	0.06	12.6	–	0.10	13.273	0.151	0.0572	0.0014	0.0753	0.0009	467.8	5.3
8.1	c	734	35	0.05	53.1	0.000031	0.34	11.876	0.101	0.0605	0.0005	0.0839	0.0007	519.5	4.3
9.1	o	597	39	0.07	38.4	0.000053	0.08	13.351	0.139	0.0570	0.0005	0.0748	0.0008	465.3	4.8
10.1	c	396	72	0.18	26.3	0.000037	0.00	12.941	0.120	0.0567	0.0006	0.0773	0.0007	479.8	4.4
11.1	c	358	32	0.09	24.7	0.000429	0.54	12.466	0.159	0.0615	0.0007	0.0798	0.0010	494.8	6.2
12.1	c	36	11	0.31	4.1	0.000475	0.37	7.541	0.135	0.0689	0.0018	0.1321	0.0024	799.9	13.9
13.1	o	796	29	0.04	51.3	–	0.04	13.327	0.112	0.0567	0.0005	0.0750	0.0006	466.2	3.9
14.1	o	243	47	0.19	15.9	0.000087	0.12	13.179	0.136	0.0574	0.0009	0.0758	0.0008	470.9	4.8
18.1	c	303	194	0.64	48.8	–	0.00	5.332	0.050	0.0765	0.0007	0.1875	0.0018	1108	10
15.1	c	673	29	0.04	44.5	0.000061	0.08	12.996	0.112	0.0573	0.0005	0.0769	0.0007	477.5	4.1
16.1	o	208	68	0.33	13.6	0.000146	<0.01	13.136	0.149	0.0560	0.0016	0.0762	0.0009	473.3	5.3

Error in FC1 Reference zircon calibration was 0.33% for the analytical session (not included in above errors but required when comparing data from different mounts).
c = core, o = oscillatory zoned overgrowths, r = rim or homogeneous patches, f = fractured or damaged grain.
[a] Uncertainties given at the one σ level.
[b] f_{206} (%) denotes the percentage of ^{206}Pb that is common Pb.
[c] Correction for common Pb made using the measured $^{238}U/^{206}Pb$ and $^{207}Pb/^{206}Pb$ ratios following Tera and Wasserburg (1972) as outlined in Williams (1998).

for the interference of ^{204}Hg and background). None of the sample revealed ^{204}Pb counts above the background level. However, the relatively high Hg signal in the gas blank does not exclude the effective presence of common Pb in the analyzed zircon. LA ICP-MS data reduction was performed using the Glitter software package (van Achterberg et al., 2001). Time-resolved isotope ratios were carefully inspected to detect perturbations related to inclusions, micro-fractures or mixing of different age domains. In all these cases, ablation intervals were set to represent only the initial unaltered portion of the signal.

Both SHRIMP and LA ICP-MS data were calculated and plotted using the program Isoplot/EX 3.0 software (Ludwig, 2003). For each zircon population, we calculated the weighted mean ages and the goodness-of-fit is reported as the mean square weighted deviation (MSWD). We added to the analytical uncertainty of the weighted means the systematic uncertainties (e.g. variation in common Pb composition, decay constant uncertainty, reference material uncertainty, and long-term variance of the mass spectrometer), which is be estimated around 2% (Horstwood et al., 2016; Spencer et al., 2016). All errors in the text and figures are given at the 2σ level.

Table 2
Summary of LA ICP-MS U–Pb isotope analyses and calculated ages for the metarhyolite of Complex II from the Torrente Visone unit (sample VAL) and for the orthogneisses from Complex II from the Nucetto massif (sample NUC). c = core, o = oscillatory zoned overgrowths, r = rim or homogeneous patches, f = fractured or damaged grain. See Supplementary Table 2 for the complete dataset.

Sample																			
NUC																			
Lat 44°21′54″N																			
Long 8° 3′24″E																			
	Spot location	Isotope ratios								Age estimates								Concordant age	
		$^{207}Pb/^{206}Pb$	1σ	$^{206}Pb/^{238}U$	1σ	$^{207}Pb/^{235}U$	1σ	$^{208}Pb/^{232}Th$	1σ	$^{207}Pb/^{206}Pb$	1σ	$^{206}Pb/^{238}U$	1σ	$^{207}Pb/^{235}U$	1σ	$^{208}Pb/^{232}Th$	1σ	Age (Ma)	2σ
z67	o/c	0.057	0.001	0.077	0.001	0.608	0.016	0.027	0.001	492	12	480	7	483	13	535	13	481	14.0
z61	o/c	0.057	0.001	0.078	0.001	0.607	0.014	0.031	0.001	476	11	482	6	482	11	623	13	482	12.0
z60	o	0.051	0.001	0.075	0.001	0.530	0.014	0.024	0.001	243	6	469	7	432	11	475	12	disc	–
z56	r	0.054	0.001	0.055	0.001	0.414	0.010	0.014	0.000	379	8	348	5	352	8	274	6	348	9.6
z56	c	0.056	0.002	0.076	0.001	0.585	0.016	0.024	0.001	469	13	471	7	467	13	487	14	470	14.0
z55	c	0.064	0.001	0.139	0.002	1.220	0.027	0.041	0.001	731	15	839	11	810	18	814	16	disc	–
z55	o/r	0.056	0.001	0.068	0.001	0.512	0.013	0.017	0.000	439	11	422	5	419	10	336	7	422	10.0
z54	o	0.056	0.001	0.071	0.001	0.538	0.012	0.020	0.000	435	10	441	6	437	10	405	9	441	11.0
z54	r	0.054	0.002	0.067	0.001	0.503	0.018	0.026	0.001	359	13	417	7	413	15	522	20	417	14.0
z43	o/r	0.055	0.001	0.067	0.001	0.515	0.013	0.022	0.001	429	10	421	6	422	11	438	11	421	12.0
z42	c	0.060	0.001	0.117	0.002	0.975	0.024	0.034	0.001	621	15	712	10	691	17	681	7	disc	–
z41	o	0.056	0.001	0.070	0.001	0.543	0.013	0.060	0.002	457	10	437	6	440	10	1172	14	437	11.0
z39	o	0.057	0.001	0.073	0.001	0.572	0.015	0.021	0.001	472	12	457	7	459	12	427	41	457	13.0
z34	o	0.054	0.001	0.077	0.001	0.576	0.015	0.022	0.001	381	9	479	7	462	12	447	12	disc	–
z33	o	0.056	0.001	0.072	0.001	0.557	0.014	0.022	0.000	458	11	447	6	449	11	439	11	448	11.0
z33	o	0.056	0.001	0.070	0.001	0.542	0.013	0.023	0.000	452	10	437	6	439	11	463	9	437	11.0
z28	o	0.056	0.001	0.072	0.001	0.555	0.013	0.026	0.001	451	10	450	6	448	11	521	10	450	12.0
z27	r	0.053	0.001	0.071	0.001	0.514	0.014	0.023	0.001	314	8	440	7	421	12	455	11	disc	–
z26	o	0.066	0.002	0.066	0.001	0.599	0.014	0.021	0.000	791	18	413	5	477	11	426	10	disc	–
z20	r	0.054	0.001	0.061	0.001	0.450	0.012	0.022	0.000	367	10	381	5	377	10	441	9	381	9.4
z20	o	0.056	0.001	0.070	0.001	0.542	0.014	0.022	0.000	445	11	439	6	440	11	437	9	439	11.0
z21	o	0.055	0.002	0.071	0.001	0.543	0.015	0.028	0.001	426	12	444	6	440	12	565	9	444	11.0
z21	o	0.057	0.002	0.073	0.001	0.569	0.018	0.027	0.001	479	15	453	7	458	14	537	16	453	13.0
z22	o	0.057	0.002	0.071	0.001	0.548	0.015	0.020	0.000	510	14	441	6	444	12	401	19	441	11.0
z24	r	0.050	0.001	0.070	0.001	0.480	0.012	0.023	0.001	198	5	434	6	398	10	452	9	disc	–
z23	o/r	0.055	0.001	0.068	0.001	0.516	0.014	0.028	0.001	420	11	423	6	422	12	558	12	423	12.0
z18	c	0.054	0.001	0.079	0.001	0.589	0.016	0.022	0.001	373	10	491	7	470	12	446	16	disc	–
z17	o	0.055	0.002	0.074	0.001	0.563	0.016	0.018	0.001	419	12	459	7	453	13	365	11	458	14.0
z17	o	0.056	0.002	0.071	0.001	0.547	0.015	0.023	0.001	444	12	443	6	443	12	464	11	443	12.0
z16	r	0.051	0.001	0.072	0.001	0.504	0.012	0.023	0.000	232	5	449	6	414	9	456	12	disc	–
z14	r	0.054	0.001	0.056	0.001	0.411	0.010	0.011	0.000	361	8	349	5	350	8	215	10	349	8.8
z14	r	0.054	0.001	0.061	0.001	0.451	0.010	0.013	0.000	374	8	379	5	378	9	252	5	379	9.5
z11	o/r	0.055	0.001	0.066	0.001	0.505	0.012	0.021	0.000	428	10	414	5	415	10	423	6	414	10.0
z10	o/r	0.055	0.001	0.067	0.001	0.506	0.012	0.018	0.000	414	9	416	5	416	9	368	8	416	10.0
z10	r	0.055	0.002	0.060	0.001	0.455	0.013	0.019	0.000	423	12	378	6	381	11	381	7	379	11.0
z4	o/r	0.055	0.001	0.068	0.001	0.517	0.012	0.021	0.000	431	10	422	5	423	10	426	9	422	10.0
z4	o	0.056	0.001	0.072	0.001	0.557	0.014	0.020	0.000	460	11	448	6	449	11	397	9	448	11.0
z2	o/r	0.056	0.002	0.068	0.001	0.521	0.014	0.021	0.001	458	12	421	5	426	12	427	9	421	10.0
z2	r	0.055	0.001	0.062	0.001	0.468	0.011	0.018	0.000	394	9	390	5	390	9	353	12	390	9.8

Sample																			
VAL																			
Lat 44°36′34″N																			
Long 8°30′54″E																			
		Isotope ratios								Age estimates								Concordant age	
		$^{207}Pb/^{206}Pb$	1σ	$^{206}Pb/^{238}U$	1σ	$^{207}Pb/^{235}U$	1σ	$^{208}Pb/^{232}Th$	1σ	$^{207}Pb/^{206}Pb$	1σ	$^{206}Pb/^{238}U$	1σ	$^{207}Pb/^{235}U$	1σ	$^{208}Pb/^{232}Th$	1σ	Age (Ma)	2σ
a3	o	0.056	0.001	0.074	0.001	0.577	0.015	0.025	0.002	467	12	461	8.2	463	11.8	496	49.6	462	11
a6	c	0.072	0.001	0.160	0.001	1.581	0.014	0.045	0.004	977	18	957	8.1	963	8.3	884	88.4	966	15
a7	r	0.056	0.002	0.067	0.001	0.526	0.016	0.021	0.002	467	13	419	8.9	429	13.1	417	41.7	disc	–
a9	o/r	0.055	0.002	0.068	0.001	0.522	0.019	0.021	0.002	409	13	427	9.1	426	15.2	413	41.3	427	12
a10	o	0.057	0.002	0.074	0.001	0.577	0.019	0.024	0.002	479	16	459	9.0	462	15.1	486	48.6	460	12
a11	c	0.061	0.002	0.102	0.001	0.854	0.021	0.031	0.003	634	22	625	8.6	627	15.5	621	62.1	626	16
a11	o	0.055	0.002	0.074	0.002	0.565	0.022	0.022	0.002	426	17	459	9.5	455	17.7	440	44.0	458	13
a12	o	0.055	0.002	0.073	0.002	0.559	0.019	0.021	0.002	417	14	456	9.3	451	15.3	421	42.1	454	13
a13	r	0.055	0.002	0.086	0.001	0.649	0.017	0.027	0.003	400	13	532	8.4	508	13.5	543	54.3	disc	–
a13	o	0.057	0.002	0.074	0.001	0.576	0.015	0.024	0.002	474	13	459	8.4	462	12.2	487	48.7	461	11
a14	o	0.060	0.002	0.072	0.001	0.590	0.019	0.024	0.002	595	18	447	9.0	471	14.9	474	47.4	disc	–
a16	o	0.057	0.001	0.072	0.001	0.560	0.015	0.022	0.002	488	12	445	8.9	452	1.2	447	44.7	disc	–
a17	c	0.071	0.002	0.068	0.001	0.660	0.016	0.049	0.005	961	22	422	8.7	515	12.8	976	97.6	disc	–
a18	r	0.055	0.001	0.071	0.001	0.542	0.013	0.023	0.002	423	9.9	443	8.5	440	10.9	457	45.7	439	9.5
a22	r	0.056	0.002	0.071	0.001	0.546	0.016	0.025	0.002	440	12	443	9.2	442	13.2	497	49.7	442	12
a23	c	0.060	0.002	0.104	0.001	0.861	0.017	0.029	0.003	614	17	635	8.5	631	12.5	568	56.8	632	16
a24	c	0.057	0.001	0.083	0.001	0.659	0.015	0.025	0.003	504	13	517	9.0	514	12.0	508	50.8	512	12
a25	r	0.057	0.002	0.069	0.001	0.540	0.016	0.024	0.002	472	13	432	9.1	438	13.3	476	47.6	disc	–
a26	c	0.059	0.002	0.080	0.002	0.655	0.023	0.044	0.004	559	22	499	9.8	511	18.3	864	86.4	501	15
a28	o	0.056	0.002	0.074	0.002	0.575	0.018	0.025	0.002	456	14	463	9.5	461	14.5	498	49.8	462	13
a29	c	0.058	0.002	0.096	0.002	0.772	0.023	0.029	0.003	541	21	589	9.8	581	17.2	582	58.2	587	17
a29	o	0.058	0.001	0.072	0.001	0.580	0.015	0.027	0.003	531	13	451	8.7	465	12.0	545	54.5	disc	–
a32	c/o	0.057	0.003	0.077	0.002	0.604	0.031	0.028	0.003	477	26	480	10.4	480	24.7	549	54.9	480	15
a33	c	0.063	0.002	0.081	0.002	0.712	0.024	0.027	0.003	723	12	504	9.9	546	18.5	532	53.2	disc	–
a34	o	0.057	0.002	0.074	0.002	0.579	0.023	0.026	0.003	491	19	458	9.8	464	18.3	510	51.0	459	14
a35	c	0.062	0.001	0.102	0.001	0.864	0.016	0.033	0.003	658	16	626	9.0	632	11.6	657	65.7	634	15
a35	o/r	0.056	0.002	0.069	0.001	0.526	0.019	0.021	0.002	446	15	428	9.2	429	15.7	410	41.0	428	12
a36	o	0.058	0.002	0.074	0.001	0.587	0.018	0.025	0.002	515	15	462	9.1	469	14.3	491	42.1	465	13
a40	o	0.055	0.002	0.074	0.002	0.562	0.023	0.022	0.002	410	16	459	9.9	453	18.4	446	44.6	458	14
a40	c	0.056	0.002	0.076	0.001	0.592	0.017	0.024	0.002	462	13	474	9.1	472	13.7	475	47.5	473	13
a41	o/r	0.056	0.001	0.070	0.001	0.542	0.015	0.024	0.002	448	11	438	9.0	440	12.5	479	47.9	440	11
a45	o	0.057	0.002	0.072	0.001	0.565	0.017	0.028	0.003	489	14	449	8.8	455	13.9	550	55.0	451	12
a51	o	0.057	0.002	0.075	0.002	0.589	0.019	0.025	0.003	495	16	465	9.6	470	15.4	499	49.9	467	13
a52	r	0.056	0.002	0.068	0.002	0.531	0.021	0.022	0.002	470	17	425	9.7	433	17.0	447	44.7	427	13
a66	o/r	0.055	0.001	0.071	0.001	0.540	0.015	0.021	0.002	426	11	441	8.8	439	12.5	420	42.0	439	11
a63	r	0.055	0.002	0.065	0.001	0.498	0.018	0.019	0.002	422	13	408	9.0	410	14.7	386	38.6	409	11
a61	o	0.056	0.002	0.072	0.001	0.556	0.018	0.024	0.002	440	13	451	9.3	449	14.4	485	48.5	450	12
a72	o/r	0.056	0.002	0.069	0.001	0.530	0.018	0.024	0.002	437	13	432	9.2	432	14.5	474	47.4	432	12
a81	o	0.055	0.002	0.074	0.002	0.568	0.022	0.022	0.002	430	17	463	9.4	457	17.9	441	44.1	461	13
a2	o	0.054	0.004	0.073	0.001	0.548	0.038	0.030	0.003	373	30	456	9.1	443	3.1	606	60.6	455	13
a3	o/r	0.057	0.005	0.071	0.002	0.550	0.046	0.024	0.002	474	18	441	10.1	445	37.5	482	48.2	441	14
a5	r	0.056	0.005	0.066	0.002	0.506	0.042	0.031	0.003	433	37	412	9.9	416	34.9	625	62.5	412	13
a8	c	0.071	0.005	0.152	0.002	1.489	0.045	0.045	0.005	964	67	915	9.7	926	27.8	892	89.2	916	27
a8	r	0.053	0.005	0.062	0.002	0.453	0.043	0.021	0.002	321	29	391	9.7	379	36.2	429	42.9	390	12
a12	o/r	0.056	0.004	0.071	0.001	0.552	0.038	0.031	0.003	470	37	442	8.6	447	30.9	621	62.1	442	12
a24	c	0.062	0.005	0.114	0.001	0.977	0.041	0.033	0.003	685	51	694	9.0	692	29.3	664	66.4	694	19
a25	o	0.056	0.005	0.073	0.001	0.556	0.042	0.024	0.002	441	38	452	9.2	449	34.3	474	47.4	452	13
a29	c/o	0.056	0.004	0.078	0.001	0.598	0.037	0.023	0.002	449	34	482	8.7	476	29.6	451	45.1	482	13
a30	c	0.064	0.006	0.122	0.002	1.063	0.055	0.046	0.005	729	68	740	10.9	735	37.7	906	90.6	740	25
a38	o/r	0.058	0.005	0.069	0.002	0.546	0.044	0.026	0.003	518	44	428	10.0	443	35.6	510	51.0	428	13

(*continued on next page*)

Table 2 (*continued*)

Sample		Isotope ratios								Age estimates						Concordant age	
		$^{207}Pb/^{206}Pb$	1σ	$^{206}Pb/^{238}U$	1σ	$^{207}Pb/^{235}U$	1σ	$^{208}Pb/^{232}Th$	1σ	$^{207}Pb/^{206}Pb$	1σ	$^{206}Pb/^{238}U$	1σ	$^{207}Pb/^{235}U$	1σ	$^{208}Pb/^{232}Th$	1σ	Age (Ma)	2σ
VAL																			
Lat 44°36′34″N																			
Long 8°30′54″E																			
a45	o	0.056	0.004	0.074	0.002	0.575	0.039	0.022	0.002	457	36	462	9.4	461	31.2	445	44.5	462	13
a50	c	0.060	0.005	0.069	0.002	0.569	0.043	0.027	0.003	610	49	428	9.9	457	34.7	531	42.1	disc	–
a53	c	0.087	0.004	0.138	0.001	1.649	0.036	0.048	0.005	1361	66	831	9.0	989	21.9	957	95.7	disc	–
a53	o	0.055	0.004	0.074	0.002	0.561	0.039	0.022	0.002	420	34	459	9.4	453	31.3	448	44.8	459	13
a63	o	0.056	0.004	0.074	0.001	0.574	0.038	0.022	0.002	468	36	460	9.0	461	30.5	441	44.1	460	13
a73	c/o	0.057	0.004	0.077	0.001	0.601	0.038	0.028	0.003	477	37	479	8.8	478	30.1	556	55.6	479	13
a76	o/r	0.056	0.004	0.069	0.001	0.530	0.039	0.023	0.002	439	35	431	8.9	432	31.6	460	46.0	431	12
a83	c	0.063	0.008	0.119	0.002	1.033	0.080	0.010	0.001	718	95	723	13.3	720	55.5	198	19.8	722	30
a78	o/r	0.056	0.004	0.071	0.001	0.544	0.037	0.027	0.003	439	18	441	8.7	441	29.9	539	53.9	441	12

4. Petrology of dated samples

4.1. Metarhyolites of Complex I

The metarhyolites I from the Calizzano massif (sample CE) are represented by two mica gneiss characterized by a layering of ribbon quartz − plagioclase K-feldspar and micas (abundant biotite and minor muscovite) (Figs. 3a, b, and 4a). K-feldspar occurs also as mm-large clasts suggesting a volcanic origin of these rocks. Accessory phases are garnet, apatite, zircon, monazite. The crystallographic orientation of medium-grained white mica and brown biotite highlights a main schistosity that locally preserve relicts of an older foliation at low angle defined by coarser-grained white mica and brown biotite (Fig. 4a–c). The metarhyolites are interbedded with Al-rich layers of paragneisses or micaschists (biotite, muscovite, quartz, plagioclase with garnet, kyanite and staurolite; Fig. 4c) and amphibolites (plagioclase + hornblende). Widespread sericite overgrowth around the K-feldspar grains and the occurrence of chlorite, epidote and stilpnomelane, particularly along late fractures cutting all previous microstructures, indicate low-temperature re-equilibration, probably related to the Alpine phases (Messiga et al., 1992; Gaggero et al., 2004).

4.2. Orthogneisses and metarhyolites of Complex II

The orthogneisses from the Calizzano and Nucetto massifs (samples CAL and NUC, respectively) show augen texture defined by K-feldspar decimetric crystals wrapped by biotite, quartz, plagioclase, medium-grained muscovite, biotite and fibrolite aligned along a single pre-Alpine (Variscan) schistosity (Fig. 3c, e, f). The Variscan schistosity of the Nucetto orthogneisses is cut by (or locally transposed along) an Alpine foliation defined by albite + Na-amphibole + pumpellyite + epidote + muscovite, indicating blueschist facies conditions (Messiga et al., 1992). In the Calizzano massif the weaker Alpine deformation and metamorphism is instead recorded by fracture cleavage and a chlorite + albite + pumpellyite paragenesis.

The metarhyolites from the Torrente Visone unit (sample VAL) show augen texture characterized by large K-feldspar phenocrysts, large to fine-grained biotite, quartz, muscovite, minor plagioclase, garnet and phengite (Figs. 3d and 4d). The metarhyolites are interbedded with mica-rich and quartzite layers. The high-P paragenesis developed along the pervasive Alpine schistosity characterizing the entire unit (Cabella et al., 1990, 1991; Cortesogno et al., 2002); rare coarse-grained muscovite and biotite define relicts of a possible older (pre-Alpine) foliation (Fig. 4d).

5. Geochronology

5.1. Zircon features

Zircon from the analyzed samples does not show significant differences between metarhyolites and orthogneisses of both Complex I and II. In all samples, in fact, zircon grains are heterogeneous in terms of size, shape, and color (Fig. 5). Crystal color varies from colorless to a wide spectrum of tones (pink, yellow, brownish); they range in length from less than 50 to 200 μm. Zircon grains exhibit mainly prismatic shape but elongate, and rounded morphology frequently occur. Crystals are often broken and/or damaged by fractures. Mineral inclusions (including apatite, rutile, and quartz) and fluid inclusions are frequently observed, particularly within the cores.

All zircon grains have xenocrystic cores surrounded by one or more secondary zircon overgrowths. The crystal cores may be structure less or with convolute-patchy zoning (Fig. 5). The

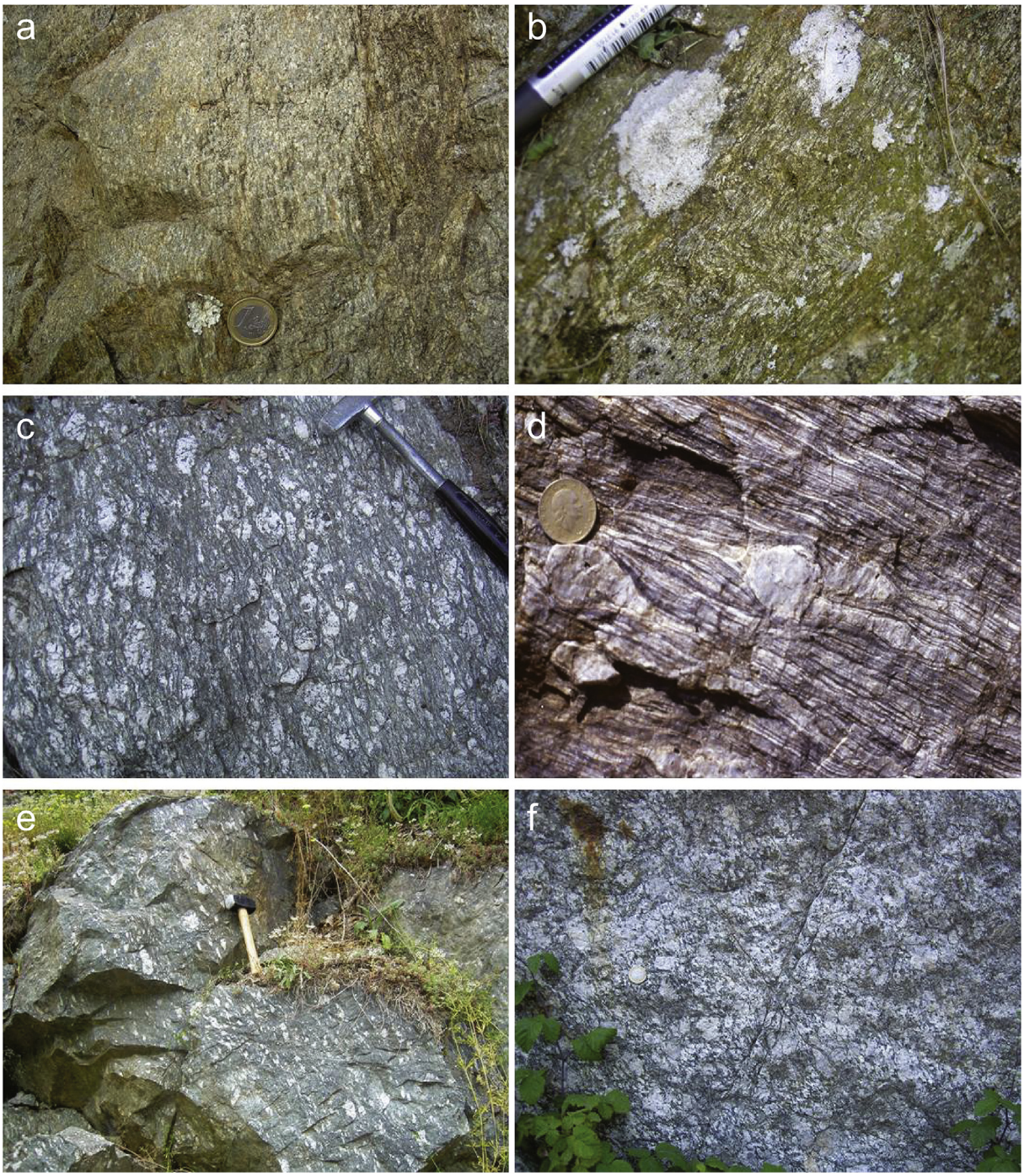

Figure 3. Mesoscopic textures of dated felsic rocks from Complex I and II. (a) Orthogneiss I (microporphyric metarhyolites) from Calizzano massif. (b) Metarhyolites (orthogneiss I) interlayered with amphibolites and paragneiss from Savona massif. (c) Coarse-grained, augen-textured orthogneiss II from the Nucetto massif. (d) Highly deformed Torrente Visone metarhyolite. (e) Sparse porphyric, large K-feldspar megacrysts orthogneiss II from Calizzano massif. (f) Intrusive orthogneiss II from Calizzano massif.

overgrowths commonly exhibit oscillatory zoning (Fig. 5), which is typical of zircon growth under igneous conditions (Corfu et al., 2003; Hoskin and Schaltegger, 2003). In the outer parts of the zircon these overgrowths may be truncated by unzoned (or with a faint zoning), poorly to highly luminescent, homogeneous patches or resorption rims (Fig. 5g–j) that are typical of low-temperature processes such as metamorphism or fluid circulation (e.g. Rubatto, 2002; Hoskin and Schaltegger, 2003).

5.2. U–Pb results

5.2.1. Metarhyolite of Complex I (Calizzano unit, Prepiedmont)

Eighteen SHRIMP spots were made on thirteen zircon grains from sample CE. All $^{206}Pb/^{238}U$ data span between 401 Ma and 1414 Ma (Table 1). The oldest dates (1414–524 Ma) are from zircon cores with complex convolute zoning or unzoned areas, while data from well preserved oscillatory zoned domains range between

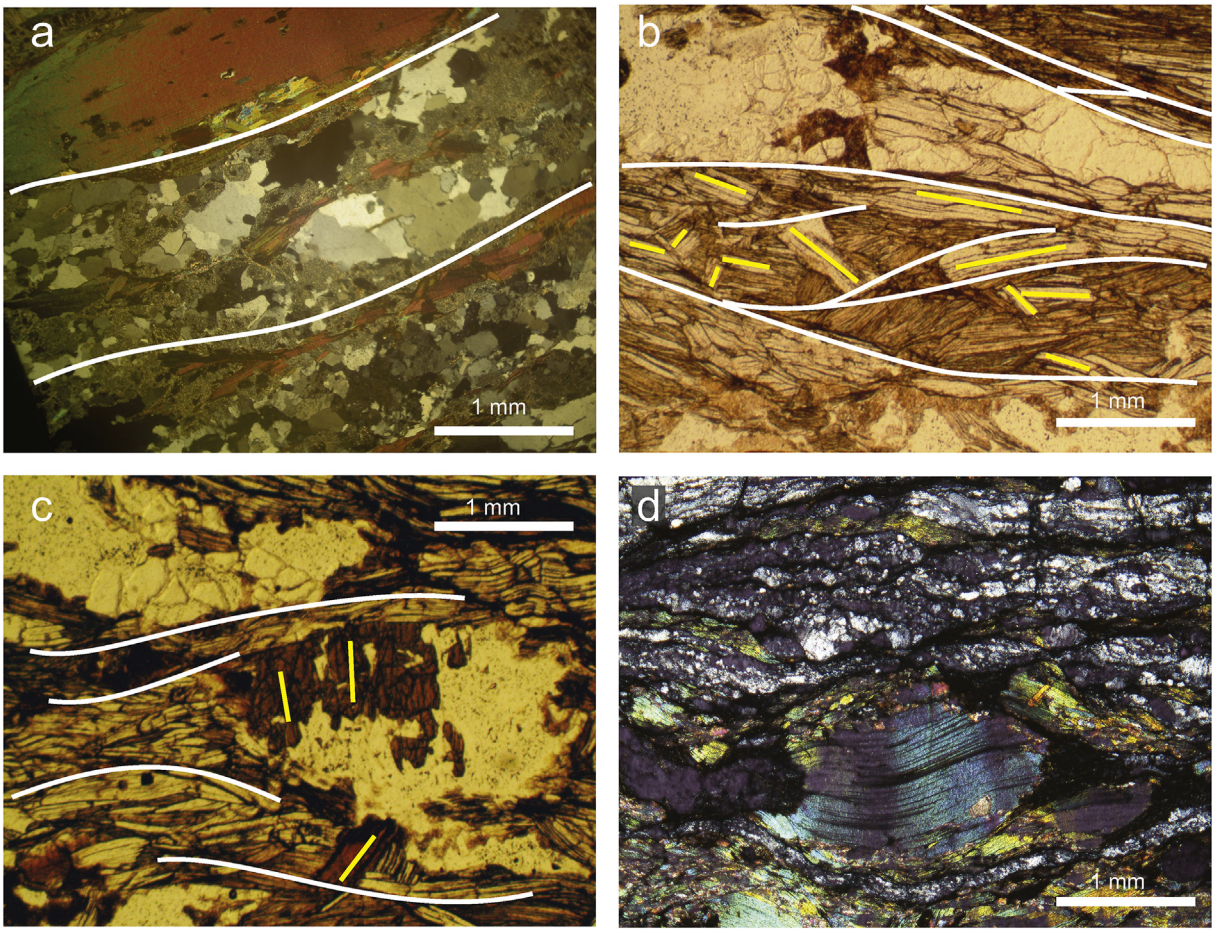

Figure 4. Cross polarized (a, d) and plane polarized (b, c) microphotographs of representative pre-Alpine foliations or relicts from the dated lithologies. (a–c) Layering of quartz and muscovite + biotite from metarhyolites of Complex I. The white lines show the main (Variscan) schistosity (foliation II), while the yellow lines highlight relicts of an older foliation (foliation I, pre-Variscan or Variscan in age) defined by different orientation of muscovite crystals. The highly variable orientation of the relicts (from sub-parallel to high-angle with respect the main foliation) reflect the transpositive character of the second deformation stage. Image (c) shows relicts of staurolite within a quartz + plagioclase clast rimmed by biotite + muscovite foliated layers. (d) Pervasive Alpine schistosity of the Torrente Visone metarhyolite. The big muscovite in the center of the photo could represents a relict of a previous (Variscan?) metamorphic stage. The attribution of the foliations to either a Variscan or Alpine deformation and metamorphic phase derives from the associated parageneses and their relationships with the map-scale structures (see text for details).

497 Ma and 519 Ma with a weighted mean $^{206}Pb/^{238}U$ age of 507 ± 15 Ma (MSWD = 1.3, probability = 0.25; Figs. 5a, b and 6a, b). The youngest ages (401–484 Ma) derive from grains fractured and/or rich of inclusions and are thus interpreted as contaminated. For this reason, they are not considered for the age calculation.

5.2.2. Orthogneiss of Complex II (Calizzano unit, Prepiedmont)

We performed nineteen SHRIMP spots on sixteen grains from sample CAL (Table 1). Data from complex convolute zoned cores show a large span between 477 Ma and 1108 Ma, with three data in the range of 477–480 Ma (Figs. 5c, d and 6c). Data from the oscillatory zoned domains range between 458 Ma and 473 Ma with a weighted mean $^{206}Pb/^{238}U$ age of 467 ± 12 Ma (MSWD = 0.8, probability = 0.63; Figs. 5c–e and 6c, d).

5.2.3. Metarhyolite of Complex II (Torrente Visone unit, Prepiedmont)

Fifty-nine laser ablation spot analyses were carried out on fifty-two zircon grains from sample VAL. Forty-nine concordant data span between 390 Ma and 966 Ma (Table 2). Complex zoned or unzoned cores have ages between 473 Ma and 966 Ma (Fig. 5f, g), while a few spots performed in the largest rims (>15–20 μm) show younger dates between 390 Ma and 442 Ma (Figs. 5g and 6e). Older ages are interpreted as inherited cores, while the youngest ones are likely related to isotopic resetting of the U–Pb system associated with metamorphic or hydrothermal events.

The oscillatory zoned domains show scattered data between 482 Ma and 427 Ma (Fig. 6e). Most of these domains are partially overlapped by narrow low luminescent patches or resorption rims, which often make difficult to discriminate between the zircon domains with the laser spot of 20 or 10 μm. In these cases, the measured isotopic ratios could be the sum of different magmatic and/or metamorphic stages, resulting in “mixed ages”, without geological meaning. However, the probability density plot shows that there is a well-defined main group for which the weighted mean age is 459 ± 12 Ma (MSWD = 0.56, probability = 0.92; Fig. 6e, f). This group is constituted by most of the best preserved oscillatory zoned domains (Fig. 5f) and its age may be assumed as representative of the crystallization time of the Torrente Visone metarhyolites.

5.2.4. Orthogneiss of Complex II (Nucetto massif, Briançonnais)

Thirty-nine laser ablation spot analyses were carried out on twenty-one zircon grains from sample NUC. Thirty-one concordant data span between 348 Ma and 481 Ma (Table 2). Three dates around 470–480 Ma and one of 441 ± 11 Ma have been measured

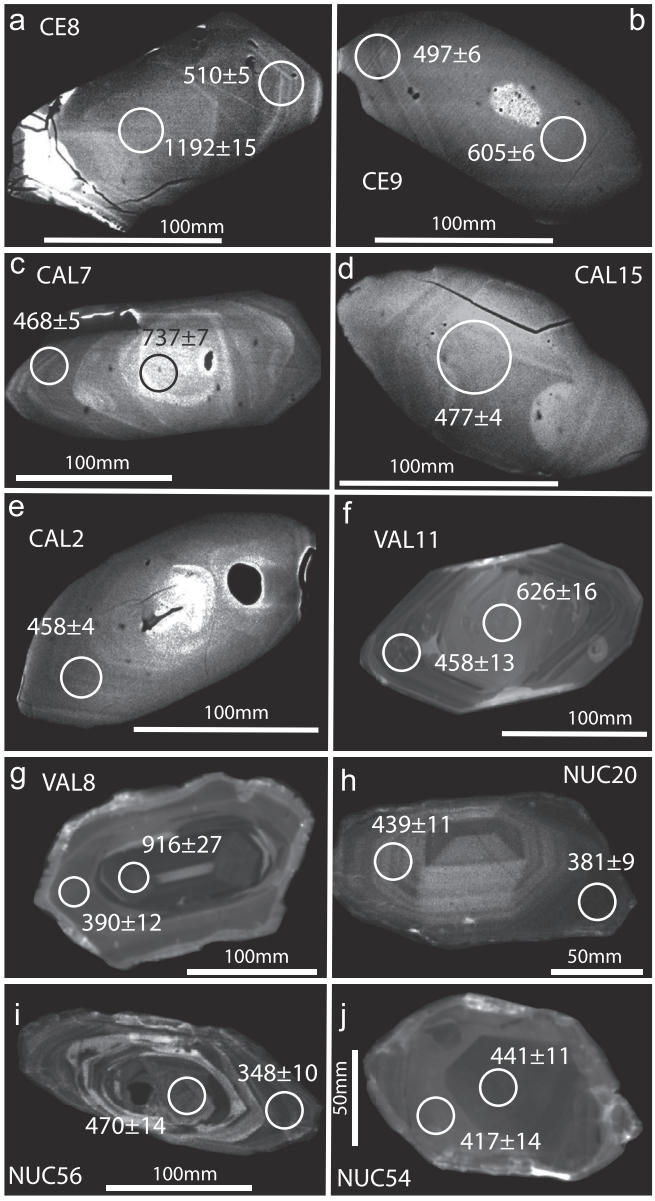

Figure 5. Cathodoluminescence images of representative zircon and analyzed spots for SHRIMP and LA-ICP-MS U–Pb dating; numbers marked on the images are the relative U–Pb dates with 2σ error.

within zircon cores (Figs. 5i and 6g), while the widest resorption rims (>20 μm) gave ages between 349 Ma and 422 Ma (Fig. 5j).

Ages older than 470 Ma are interpreted as inherited cores, while the youngest data are considered related to late stage isotopic resetting of the U–Pb system.

The oscillatory zoned domains show ages scattered between 348 Ma and 458 Ma. Also in this sample, most of these domains are truncated or partially overlapped by low luminescent patches or resorption rims (Fig. 5h–j). This large pattern could be influenced by the complex 3D crystal structure that often prevents to correctly discriminate among the zircon domains with the laser spot. These considerations suggest that this wide pattern may incorporate "mixed ages" without geological meaning. However, the data distribution shows two main groups at 410–430 Ma and 430–460 Ma, the older of which is constituted by the best preserved oscillatory zoned domains (Fig. 5h), whereas the younger one includes some dates from the wide rims (Fig. 6g). This suggests that the data of the younger group are partially influenced by low temperature processes that generated the resorption rims. We thus assume the weighted mean age of 445.5 ± 12 Ma (MSWD = 1.4, probability = 0.18; Fig. 6h) calculated from the older group as the most probable crystallization age of the magmatic protolith of the Nucetto orthogneisses.

6. Discussion

6.1. Timing of the igneous events

The new U–Pb ages from four samples are representative of the best-exposed outcrops of the intrusive and volcanic acidic rocks of the two pre-Variscan lithologic complexes, and are thus the best samples to describe the main magmatic phases of the Early Paleozoic history of the Ligurian basements. All analyzed samples show zircon grains with cores that can be unzoned or characterized by complex convolute zoning. These structures are typical of xenocrystic cores and their ages are systematically older than the surrounding overgrowths. However, one single zircon core shows a considerably younger data (441 Ma; Fig. 5j); as evidenced by the thick resorption rim enveloping the grain, this zircon was affected by an important recrystallization that probably partially contaminated also the core. The xenocrystic cores from the metarhyolites of Complex I (sample CE) have Mesoproterozoic to lower Cambrian ages, while in the orthogneisses and metarhyolites of the Complex II (samples CAL, VAL and NUC) cores as young as ~470–480 Ma have been found. These data indicate that the zircon cores record the previous igneous events. For example, the youngest sample (VAL from the Torrente Visone metarhyolites II) shows a data distribution that includes age representative of both Complex I metarhyolites (sample CE) and the Complex II orthogneisses (sample CAL). This suggests that each igneous event recycles rocks previously emplaced during the different magmatic pulses.

Around the inherited cores, zircon crystals show oscillatory zoned domains that are typical of crystallization under igneous conditions (Corfu et al., 2003; Hoskin and Schaltegger, 2003). When these domains are well developed and far from resorption rims, the relative dates cluster in narrow intervals (<30 Ma; Fig. 6a, c), the weighted mean of which likely represents the crystallization age of the relative igneous body (507 ± 15 Ma and 467 ± 12 Ma for samples CE and CAL, respectively; Fig. 6b, d). On the contrary, when the oscillatory zoned overgrowths are closely associated with rims or patches that partially or completely contaminate the original magmatic structures (samples VAL and NUC), the data scatter over a large interval (up to 130 Ma; Fig. 6e, f). In these samples, however, the age distributions show a main group constituted by the best preserved magmatic structures and characterized by a narrow peak (Fig. 6e, f), the relative weighed means of which are interpreted as the most probable crystallization ages (459 ± 12 Ma and 445.5 ± 12 Ma for samples VAL and NUC, respectively). The other younger data from the oscillatory zoned domains probably reflect the disturbance associated with rims. When measurable (>15–20 μm), in fact, the resorption rims show ages partially overlapping the youngest data measured from the oscillatory zoned domains (Fig. 6e, f) and likely represent late-stage isotopic resetting of the U–Pb system during the pre-Variscan or Variscan thermal (igneous or metamorphic) events.

6.2. The Cambrian–Ordovician evolution of the Ligurian Alps basements in the frame of the northern Gondwana margin

The new geochronological investigations provided by this study integrated with the literature data reveal that the pre-Variscan

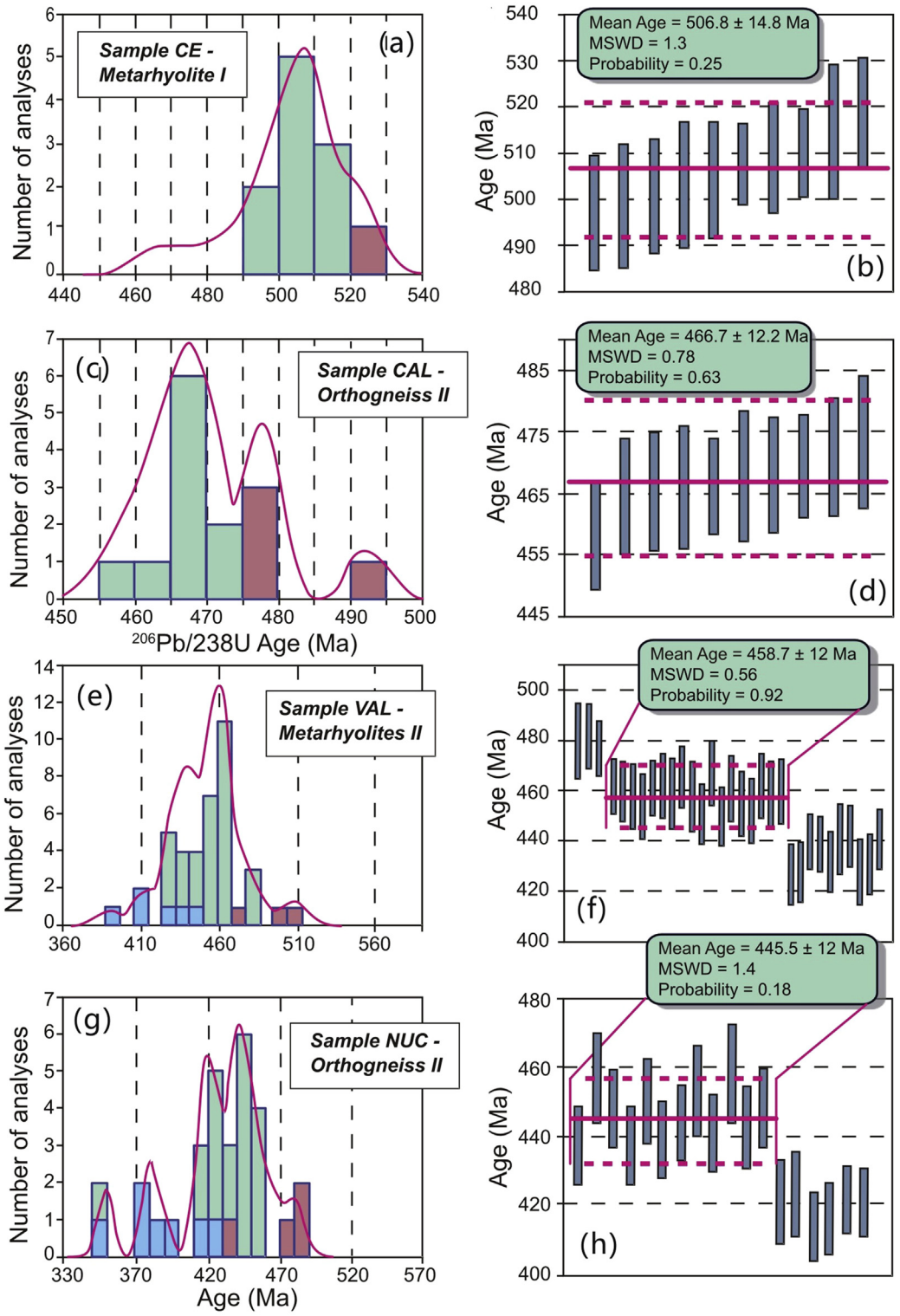

Figure 6. Probability density plot and U–Pb weighted mean ages of the analyzed samples (the error reported is the sum of the analytical and systematic errors; see Spencer et al., 2016). Red, green and blue boxes indicate results from inherited cores, magmatic oscillatory overgrowths and rims, respectively. The inherited cores older than ~540 Ma are not plotted.

igneous rocks of the Ligurian basements were emplaced during multiple igneous episodes during the Cambrian–Silurian times.

The meta-effusive rocks of the Complex I (metarhyolites and amphibolites) represent the record of a bimodal magmatism (calc-alkaline rhyolites and tholeiitic basalts; Cortesogno et al., 1993, 1997; Gaggero et al., 2004) interstratified within a thick pelitic-arenitic sequence (now paragneisses and micaschists). This bimodal activity suggests an extensional regime but only a few occurrences of mantle-derived ultramafic bodies (Cortesogno et al., 1993) document for a possible oceanization; it is more likely that just an intracontinental rifting was produced. The age of basaltic emplacement in Liguria is unknown, while the new age of 507 ± 15 Ma of the metarhyolite I

represents the crystallization age of the widest metarhyolite body of the Complex I. This age is slightly older than the isotope dilution TIMS U–Pb zircon age of 494 ± 5 Ma (Molina, 2002) performed on the orthogneisses I, which were the granitoids intruded within the volcano-sedimentary succession (Cortesogno et al., 1993).

Several mafic and ultramafic associations involved in similar volano-sedimentary sequences, have been dated between 530 Ma and 500 Ma in the neighboring Alpine basements, and considered as ophiolitic sequences emplaced during a Cambrian extensional regime (e.g. Ménot et al., 1988; Müller et al., 1996; Schaltegger et al., 2002; Bussien et al., 2011). At this time, extensional setting is a common feature of the other basements located along the northern Gondwana margin; the formation of rift basins characterized by bimodal magmatism is indeed documented in Iberia, Corsica-Sardinia and Bohemian massif (e.g. Paquette et al., 1989; Linnemann et al., 2008; Oggiano et al., 2010; Gaggero et al., 2012; Sánchez-Martínez et al., 2012). The Calabria-Peloritani block records instead only Late Proterozoic ages of syn-orogenic metamorphism and magmatism (ca. 579–543 Ma; Williams et al., 2012; Fiannacca et al., 2013; Fornelli et al., 2016), without evidences of Cambrian igneous activity. This extensional setting has been interpreted either as resulting from back-arc rifting (Chamrousse event; Guillot et al., 2002; von Raumer and Stampfli, 2008) or as thinning of the lithosphere and upwelling of asthenosphere through slab-windows formed by subduction of an earlier mid-oceanic ridge (Iapetus-Tornquist Ocean; Linnemann et al., 2007, 2008).

The igneous rocks of the Complex I (ages older than ~490 Ma) were folded together with the terrigenous sediments (i.e. their host) prior to be intruded by large volumes of manly acidic and minor mafic rocks of the Complex II, which were emplaced between 467 ± 12 Ma and 445.5 ± 12 Ma (this study; Molina, 2002; Giacomini et al., 2007). The existence of a tectono-metamorphic cycle predating the Complex II emplacement is suggested not only by field relationships (Seno et al., 2010) but also by the preservation in Complex I of relicts of an older schistosity with amphibolite facies conditions (Gaggero et al., 2004 and references within). As such, we should speculate a subduction or collisional setting to justify these conditions. A possible Late Cambrian–Early Ordovician subduction cycle is supported by the 478 ± 5 Ma age of the metamorphism in the External massif (Schaltegger et al., 2003). However, relicts of this metamorphic phase were not found along other northern Gondwana blocks (e.g. Sardinia and Calabria-Peloritani), thus questioning the nature and extension of this metamorphic event (e.g. Oggiano et al., 2010; Fornelli et al., 2016). Furthermore, because of the pervasive Variscan deformation and recrystallization, it is impossible to demonstrate a direct correlation between these foliation relicts and the large-scale folding affecting the Complex I sequence. We cannot thus exclude that the poorly preserved foliation I could instead represent just an early stage of the Variscan metamorphic cycle, rather than a pre-Variscan event. In this case, the folding event characterizing the Complex I should be interpreted as a deformation event without metamorphism; as such, it can be correlated with the Sardic phase of Sardinia (marked by a key angular unconformity between a folded Cambrian volcano-sedimentary sequence and a Middle Ordovician volcanic cycle; Martini et al., 1991; Oggiano et al., 2010).

The dated rocks of Complex II (between ~467 ± 12 Ma and 445.5 ± 12 Ma) are representative of the huge volumes of pre-aluminous S-type granitoids, rhyolites and minor MORB-gabbros and rare basic to intermediate dykes, which represent a calc-alkaline suite emplaced in the Ligurian basements before the Variscan Cycle. Comparable Ordovician magmatic suites of calc-alkaline granitoids and volcanites, associated with minor volumes of mafic rocks are documented between ~480 Ma and ~450 Ma in most Alpine basements (Bussy and von Raumer, 1994; Poller et al., 1997; Schaltegger and Gebauer, 1999; Bertrand et al., 2000; Bussy et al., 2000, 2011; Rubatto et al., 2001; Guillot et al., 2002; von Raumer et al., 2002;Schaltegger et al., 2003; Schulz et al., 2008; Bussien et al., 2011), Corsica-Sardinia (Giacomini et al., 2006; Oggiano et al., 2010; Gaggero et al., 2012), Montagne Noir (Roger et al., 2004), Pyrenees (e.g. Deloule et al., 2002; Castiñeiras et al., 2008; Casas et al., 2010, 2011; Navidad et al., 2010; Liesa et al., 2011), Iberia (e.g. Valverde-Vaquero and Dunning, 2000; Gutiérrez-Alonso et al., 2007; Montero et al., 2007; Díez Montes et al., 2010; Navidad and Castiñeiras, 2011; Rubio-Ordóñez et al., 2012), Saxothuringia (Linnemann et al., 2000; Winchester et al., 2003) and Calabro-Peloritani Arc (e.g. Micheletti et al., 2007, 2011; Fiannacca et al., 2008; Fornelli et al., 2016). This distribution argues for the presence of an active margin associated with the subduction of an ocean (the Rheic Ocean) beneath the northern Gondwana margin, where the huge calc-alkaline intrusions were emplaced (e.g. von Raumer and Stampfli, 2008; von Raumer et al., 2013).

6.3. The Late Ordovician-Silurian thermal event

The age of 445.5 ± 12 Ma from the orthogneisses II (early S-type monzogranites; Gaggero et al., 2004) of the Briançonnais basement (Nucetto massif) is considerably younger than the other data from the Complex II. It is the first report of Late Ordovician–Early Silurian age from the Penninic basements of the Alps. However, a few anatectic bodies, calc-alkaline or alkaline acidic volcanites, andesites and gabbros with ages in ranges of 450–430 Ma have been found in several places, including the External Massifs (Paquette et al., 1989; Rubatto et al., 2001; Schaltegger et al., 2003; Schulz and von Raumer, 2011), Austroalpine and Carnic Alps (Schulz et al., 2008; Thöny et al., 2008; Rode et al., 2012), Calabria-Peloritani (Trombetta et al., 2004) Sardinia (Oggiano et al., 2010) and Pyrenees (Casas et al., 2010). In Sardinia, the Silurian igneous activity has alkaline character and is represented by dikes and sills that allow defining a distinct igneous activity from the arc-related bimodal magmatism (Oggiano et al., 2010; Gaggero et al., 2012). This thermal event occurred under extensional regime possibly following the collapse of the Mid-Ordovician arc (Oggiano et al., 2010) and it was likely related to the initial rifting of Paleotethys (von Raumer and Stampfli, 2008; Stampfli et al., 2011).

The magmatic domains of zircon from the analyzed samples are often truncated by the growth of wide rims (Fig. 4) that show a considerable number of data scattered between ~440 Ma and ~345 Ma (Tables 1 and 2; Fig. 5). These dates may record distinct thermal perturbations associated with (i) a persistence of the rifting-related magmatism during the Silurian (i.e. the peak around ~420 Ma of Fig. 5e, g), (ii) followed by the different stages of the Variscan orogenic phases (ages <420 Ma).

7. Conclusions

The pre-Mesozoic basements of the Ligurian Alps are dismembered into several units by the Alpine deformation. However, the Alpine metamorphic phases developed low-*T* parageneses, thus preserving high-*T* relicts of the pre-Variscan and Variscan igneous and/or metamorphic phases. New geochronological data indicate that a complete record of Cambrovician-Silurian magmatism is still preserved in the Ligurian basements. SHRIMP and LA-ICP MS U–Pb data suggest that the main igneous products characterizing the two lithostratigraphic complexes (Complexs I and II) were emplaced through several magmatic pulses. Effusive and intrusive products of Complex I are dated in the middle–upper Cambrian (507 ± 15 Ma to 494 ± 5 Ma). Analogues from Sardinia and Alps are referred to the rifting phase at

the northern Gondwana margin, with evidence of progression from south northwards in present coordinates.

Complex II rocks outpoured or intruded the crust from the Early Ordovician toward the Silurian (473 ± 1 Ma, 468 ± 1 Ma, 467 ± 12 Ma, 459 ± 3 Ma and 445 ± 12 Ma). This age span is ascribed to the evolution of an arc system, assessed in adjacent peri-gondwanian terranes. In particular, the Late Ordovician–Silurian igneous activity could be interpreted as the onset of the Silurian post-arc activity or as a prolongation of the Mid Ordovician arc.

Both Complexs I and II are characterized by a main pervasive schistosity (foliation II), associated with the Variscan structure and parageneses and dated between 420 Ma and 300 Ma (Del Moro et al., 1981; Barbieri et al., 2003; Giacomini et al., 2007). However, intrusives of Complex II cut a previously folded crust made of the Complex I sequence, thus highlighting a deformational event between the emplacement of the two complexes (i.e. between ~494 Ma and 473 Ma). However, it is not clear if this deformational event was associated with a pre-Variscan schistosity (foliation I) rarely preserved only in the rocks of Complex I. While in the External Massifs of the Alps a subduction cycle is documented at this time, other blocks of the northern Gondwana margin record only non-metamorphic deformation (e.g. the Sardic phase; Oggiano et al., 2010). Available data from the Ligurian segment cannot discriminate between this two model, therefore the geodynamic interpretation of the Cambrovician–Ordovician transition remains problematic. However, the new geochronological data indicate that the emplacement of huge magmatic (mainly calc-alkaline) volumes through discrete pulses during the Cambrian–Silurian, is a key feature of the Ligurian block, as well as the other sectors constituting the northern Gondwana margin (e.g. Corsica-Sardinia, Pyrenees, Iberia, Calabria-Peloritani, Bohemian Massif). This magmatism may be referred to as an Andean type arc – with the subduction of the Rheic Ocean beneath the northern Gondwana margin – evolving toward a rifting stage related to the initial rifting of Paleotethys. This study thus confirms the affinity of the Ligurian basements with the other sectors of the northern margin of Gondwana that evolved through several steps of rifting and subduction before the starting of the Variscan cycle.

Acknowledgments

This research was supported by Italian 1:50,000 Geological Mapping (CARG—Regione Liguria Project, University of Pavia grants). Editorial Assistant Dr. Lily Wang, Handling Editor Dr. C.J. Spencer, two reviewers G. Oggiano, F. Micheletti and an anonymous reviewer are gratefully acknowledged for substantial revisions and constructive suggestions that greatly improved the paper.

Appendix A. Supplementary data

Supplementary data related to this article can be found at https://doi.org/10.1016/j.gsf.2018.01.003.

References

Barbieri, C., Carrapa, B., Di Giulio, A., Wijbrans, J., Murrel, G.R., 2003. Provenance of Oligocene synorogenic sediments of the Ligurian Alps (NW Italy): inferences on belt age and cooling history. International Journal of Earth Sciences 92, 758–778.

Bertrand, J.-M., Pidgeon, R.T., Leterrier, J., Guillot, F., Gasquet, D., Gattiglio, M., 2000. SHRIMP and IDTIMS U–Pb zircon ages of the pre-Alpine basement in the Internal Western Alps (Savoy and Piemont). Schweizerische Mineralogische Petrographische Mitteilungen 80, 225–248.

Bussien, D., Bussy, F., Magna, T., Masson, H., 2011. Timing of Palaeozoic magmatism in the Maggia and Sambucco nappes and paleogeographic implications (Central Lepontine Alps). Swiss Journal of Geosciences 104, 1–29. https://doi.org/10.1007/s00015-010-0049-6.

Bussy, F., von Raumer, J., 1994. U-Pb geochronology of Palaeozoic magmatic events in the Mont-Blanc Crystalline Massif, Western Alps. Schweizerische Mineralogische und Petrographische Mitteilungen 74, 514–515.

Bussy, F., Derron, M., Jacquod, J., Thélin, P., Sartori, M., 1996. The 500 Ma-old Thyon metagranite: a new A-type granite occurrence in the penninic realm (Western Alps, Switzerland). European Journal of Mineralogy 8, 565–575.

Bussy, F., Hernández, J., Von Raumer, J., 2000. Bimodal magmatism as a consequence of the post-collisional readjustment of the thickened variscan continental lithosphere (Aiguilles Rouges/Mont-Blanc massifs, western Alps). Transactions Royal Society of Edinburgh 91, 221–233.

Bussy, F., Péronnet, V., Ulianov, A., Epard, J.L., von Raumer, J., 2011. Ordovician magmatism in the external French Alps: witness of a peri-Gondwanan active continental margin. In: Gutiérrez-Marco, J.C., Rábano, I., García-Bellido, D. (Eds.), The Ordovician of the World, vol. 14. Instituto Geológico y Minero de España, Cuadernos del Museo Geominero, Madrid, pp. 75–82.

Cabella, R., Cortesogno, L., Gaggero, L., 1990. Il basamento cristallino del Torrente Visone. Rendiconti della Società Geologica Italiana 14, 29–33.

Cabella, R., Cortesogno, L., Dallagiovanna, G., Gaggero, L., Lucchetti, L., 1991. Metamorfismo alpino a giadeite + quarzo in crosta continentale nel Brianzonese ligure. Atti Ticinensi di Scienze della Terra 34, 43–54.

Casas, J.P., Castiñeiras, P., Navidad, M., Liesa, M., Carreras, J., 2010. New insights into the Late Ordovician magmatism in the Eastern Pyrenees: U-Pb SHRIMP zircon data from the Canigó Massif. Gondwana Research 17, 317–324. https://doi.org/10.1016/j.gr.2009.10.006.

Casas, J.P., Castiñeiras, P., Navidad, M., Liesa, M., Martinez, J.F., Carreras, J., Reche, J., Iriondo, A., Aleinikoff, J., Cirés, J., Dietsch, C., 2011. Ordovician magmatism in NE Iberia. In: Gutiérrez-Marco, J.C., Rábano, I., García-Bellido, D. (Eds.), The Ordovician of the World, vol. 14. Instituto Geológico y Minero de España, Cuadernos del Museo Geominero, Madrid, pp. 95–100.

Castiñeiras, P., Navidad, M., Liesa, M., Carreras, J., Casas, J.M., 2008. U-Pb zircon ages (SHRIMP) for Cadomian and Early Ordovician magmatism in the Eastern Pyrenees: new insights into the pre-Variscan evolution of the northern Gondwana margin. Tectonophysics 461, 228–239. https://doi.org/10.1016/j.tecto.2008.04.005.

Casini, L., Cuccuru, S., Maino, M., Oggiano, G., Tiepolo, M., 2012. Emplacement of the Arzachena Pluton (Corsica-Sardinia Batholith) and the geodynamics of incoming Pangaea. Tectonophysics 544–545, 31–49. https://doi.org/10.1016/j.tecto.2012.03.028.

Casini, L., Cuccuru, S., Maino, M., Oggiano, G., Puccini, A., Rossi, P., 2015a. Structural map of Variscan northern Sardinia (Italy). Journal of Maps 11 (1), 75–84. https://doi.org/10.1080/17445647.2014.936914.

Casini, L., Cuccuru, S., Puccini, A., Oggiano, G., Rossi, P., 2015b. Evolution of the Corsica–Sardinia Batholith and late-orogenic shearing of the Variscides. Tectonophysics 646, 65–78. https://doi.org/10.1016/j.tecto.2015.01.017.

Corfu, F., Hanchar, J.M., Hoskin, P.W.O., Kinny, P., 2003. Atlas of zircon textures. In: Hanchar, J.M., Hoskin, P.W.O. (Eds.), Zircon, Mineralogical Society of America. Reviews in Mineralogy and Geochemistry vol. 53, 468–500.

Cortesogno, L., 1986. Magmatismo e metamorfismo pre-Alpini nel basamento e nel tegumento delle Alpi Liguri. Memorie della Società Geologica Italiana 28, 331–352.

Cortesogno, L., Dallagiovanna, G., Gaggero, L., Vanossi, M., 1993. Elements for the Palaeozoic history of the Ligurian Alps. In: von Raumer, J., Neubauer, D. (Eds.), Pre-Alpine Geology. Springer Verlag, pp. 258–276.

Cortesogno, L., Gaggero, L., Capelli, C., 1997. Petrology of pre-Alpine eclogites and amphibolites from the Ligurian Briançonnais basement. Atti Ticinensi di Scienze della Terra 39, 3–29.

Cortesogno, L., Gaggero, L., Lucchetti, G., Cabella, R., 2002. Composition and miscibility gap in Na–Ca clinopyroxenes through high-pressure metamorphism. Periodico di Mineralogia 71, 1–25.

Cortesogno, L., Gaggero, L., Oggiano, G., Paquette, J.L., 2004. Different tectono-thermal evolutionary paths in eclogitic rocks from the axial zone of the Variscan chain in Sardinia (Italy) compared with the Ligurian Alps. Ofioliti 29, 125–144.

Cruciani, G., Franceschelli, M., Langone, A., Puxeddu, M., Scodina, M., 2015. Nature and age of pre-Variscan eclogite protoliths from the Low-to Medium-Grade Metamorphic Complex of north–central Sardinia (Italy) and comparisons with coeval Sardinian eclogites in the northern Gondwana context. Journal of the Geological Society 172 (6), 792–807.

Dallagiovanna, G., Gaggero, L., Maino, M., Seno, S., Tiepolo, M., 2009. U-Pb zircon ages for post-Variscan volcanism in the Ligurian Alps (Northern Italy). Journal of the Geological Society of London 166, 1–14. https://doi.org/10.1144/0016-76492008-027.

Decarlis, A., Dallagiovanna, G., Lualdi, A., Maino, M., Seno, S., 2013. Stratigraphic evolution in the Ligurian Alps between Variscan heritages and the Alpine Tethys opening: a review. Earth-Science Reviews 125, 43–68. https://doi.org/10.1016/j.earscirev.2013.07.001.

Decarlis, A., Maino, M., Dallagiovanna, G., Lualdi, A., Masini, E., Toscani, G., Seno, S., 2014. Salt tectonics in the SW Alps (Italy–France): from rifting to the inversion of the European continental margin in a context of oblique convergence. Tectonophysics 636, 293–314. https://doi.org/10.1016/j.tecto.2014.09.003.

Decarlis, A., Felli, M.G., Maino, M., Ferrando, S., Manatschal, G., Gaggero, L., Seno, S., Stuart, F.M., Beltrando, M., 2017. Tectono-thermal evolution of a distal rifted margin: constraints from the Calizzano Massif (Prepiedmont-Briançonnais domain, Ligurian Alps). Tectonics 36. https://doi.org/10.1002/2017TC004634.

Del Moro, A., Pardini, G., Messiga, B., Poggio, M., 1981. Dati petrologici e radiometrici preliminari sui massicci cristallini della Liguria occidentale. Rendiconti della Società Italiana di Mineralogia e Petrologia 38, 73–87 (in Italian).

Deloule, E., Alexandrov, P., Cheilletz, A., Laumonier, B., Barbey, P., 2002. In situ U-Pb zircon ages for Early Ordovician magmatism in the eastern Pyrenees, France: the Canigou orthogneisses. International Journal of Earth Sciences 91, 398–405. https://doi.org/10.1007/s00531-001-0232-0.

Desmons, J., Compagnoni, R., Cortesogno, L., Frey, M., Gaggero, L., 1999a. Pre-Alpine metamorphism of the internal zones of the Western Alps. Schweizer Mineralogische und Petrographische Mitteilungen 79, 23–39.

Desmons, J., Aprahamian, J., Compagnoni, R., Cortesogno, L., Frey, M., Gaggero, L., Dallagiovanna, G., Seno, S., 1999b. Alpine metamorphism of the Western Alps: I. Middle to high T/P metamorphism. Schweizerische Mineralogische und Petrographische Mitteilungen 79, 89–110.

Díez Montes, A., Martínez Catalán, J.R., Bellido Mulas, F., 2010. Role of the Ollo de Sapo massive felsic volcanism of NW Iberia in the Early Ordovician dynamics of northern Gondwana. Gondwana Research 17, 363–376. https://doi.org/10.1016/j.gr.2009.09.001.

Elliot, D.H., Fanning, C.M., Laudon, T.S., 2016. The Gondwana plate margin in the Weddell sea sector: zircon geochronology of upper paleozoic (mainly permian) strata from the Ellsworth mountains and eastern Ellsworth land, Antarctica. Gondwana Research 29, 234–247. https://doi.org/10.1016/j.gr.2014.12.001.

Fiannacca, P., Williams, I.S., Cirrincione, R., Pezzino, A., 2008. Crustal contributions to Late Hercynian peraluminous magmatism in the southern Calabria–Peloritani Orogen, southern Italy: petrogenetic inferences and the Gondwana connection. Journal of Petrology 49 (8), 1497–1514.

Fiannacca, P., Williams, I.S., Cirrincione, R., Pezzino, A., 2013. The augen gneisses of the Peloritani Mountains (NE Sicily): granitoid magma production during rapid evolution of the northern Gondwana margin at the end of the Precambrian. Gondwana Research 23 (2), 782–796.

Fornelli, A., Micheletti, F., Piccarreta, G., 2016. Late-Proterozoic to Paleozoic history of the peri-Gondwana Calabria–Peloritani terrane inferred from a review of zircon chronology. SpringerPlus 5 (1), 1–19. https://doi.org/10.1186/s40064-016-1839-8.

Franke, W., Robin, M., Cocks, L., Torsvik, T.H., 2017. The Palaeozoic Variscan oceans revisited. Gondwana Research 48, 257–284. https://doi.org/10.1016/j.gr.2017.03.005.

Gaggero, L., Cortesogno, L., Bertrand, J.M., 2004. The pre-Namurian basement of the Ligurian Alps: a review of the lithostratigraphy, pre-Alpine metamorphic evolution, and regional comparisons. Periodico di Mineralogia, Special Issue 2 (73), 85–96.

Gaggero, L., Oggiano, G., Funedda, A., Buzzi, L., 2012. Rifting and arc-related early Palaeozoic volcanism along the north Gondwana margin: geochemical and geological evidence from Sardinia (Italy). The Journal of Geology 120, 273–292. https://doi.org/10.1086/664776.

Gaggero, L., Gretter, N., Langone, A., Ronchi, A., 2017. U-Pb geochronology and geochemistry of late Palaeozoic volcanism in Sardinia (southern Variscides). Geoscience Frontiers 8 (6), 1263–1284. https://doi.org/10.1016/j.gsf.2016.11.015.

Giacomini, F., Bomparola, R.M., Ghezzo, C., Guldbransen, H., 2006. The geodynamic evolution of the Southern European Variscides: constraints from the U/Pb geochronology and geochemistry of the lower Palaeozoic magmatic-sedimentary sequences of Sardinia (Italy). Contributions to Mineralogy and Petrology 152 (1), 19–42.

Giacomini, F., Braga, R., Tiepolo, M., Tribuzio, R., 2007. New constraints on the origin and age of Variscan eclogitic rocks (Ligurian Alps, Italy). Contributions to Mineralogy and Petrology 153, 29–53.

Guillot, F., Liegeois, J.-P., Fabre, J., 1991. Upper Cambrian granophyre of Mount Pourri, Brianconnais Zone, Vanoise; first U/Pb dating of zircon from the basement of the internal French Alps. Comptes Rendus de l'Académie des Sciences, Paris 313 (II), 239–244.

Guillot, F., Schaltegger, U., Bertrand, J.M., Deloule, E., Baudin, T., 2002. Zircon U-Pb geochronology of Ordovician magmatism in the polycyclic Ruitor massif (Internal W Alps). International Journal of Earth Sciences 91, 964–978.

Gutiérrez-Alonso, G., Fernández-Suárez, J., Gutiérrez-Marco, J.C., Corfu, F., Murphy, J.B., Suárez, M., 2007. U-Pb depositional age for the upper Barrios Formation (Armorican quartzite facies) in the Cantabrian zone of Iberia: implications for stratigraphic correlation and paleogeography. In: Linnemann, U., Nance, R.D., Kraft, P., Zulauf, G. (Eds.), The Evolution of the Rheic Ocean: From Avalonian-Cadomian Active Margin to Alleghenian-Variscan Collision, Geological Society of America, Special Paper, vol. 423, pp. 287–296.

Horstwood, S.A., Foster, G.L., Parrish, R.R., Noble, S.R., Nowell, G.M., 2003. Common-Pb corrected in situ U–Pb accessory mineral geochronology by LA–MC–ICP–MS. Journal of Analytical Atomic Spectrometry 18, 837–846.

Horstwood, M.S., Košler, J., Gehrels, G., Jackson, S.E., McLean, N.M., Paton, C., …,Bowring, J.F., 2016. Community-derived standards for LA-ICP-MS U-(Th-) Pb geochronology–uncertainty propagation, age interpretation and data reporting. Geostandards and Geoanalytical Research 40 (3), 311–332. https://doi.org/10.1111/j.1751-908X.2016.00379.x.

Hoskin, P.W.O., Schaltegger, U., 2003. The composition of zircon and igneous and metamorphic petrogenesis. In: Zircon, Hanchar, J.M., Hoskin, W.O. (Eds.), Reviews in Mineralogy and Geochemistry, vol. 53. Mineralogical Society of America, pp. 7–62.

Ketchum, J.W.F., Jackson, S.E., Culshaw, N.G., Barr, S.M., 2001. Depositional and tectonic setting of the Palaeoproterozoic Lower Aillik Group, Makkovik Province, Canada: evolution of a passive margin–foredeep sequence based on petrochemistry and U–Pb (TIMS and LAM–ICP–MS) geochronology. Precambrian Research 105, 331–356.

Lemoine, M., Bas, T., Arnaud-Vanneau, A., Arnaud, H., Dumont, T., Gidon, M., Bourbon, M., de Graciansky, P.-C., Rudkiewicz, J.-L., Mégard-Galli, J., Tricart, P., 1986. The continental margin of the Mesozoic Tethys in the Western Alps. Marine and Petroleum Geology 3, 179–199.

Liesa, M., Carreras, J., Castiñeiras, P., Casas, J.M., Navidad, M., Vilà, M., 2011. U-Pb zircon age of Ordovician magmatism in the Albera Massif (Eastern Pyrenees). Geológica Acta 9, 93–101.

Linnemann, U., Gehmlich, M., Tichomirowa, M., Buschmann, B., Nasdala, L., Jonas, P., Lützner, H., Bombach, K., 2000. From Cadomian subduction to early Palaeozoic rifting: the evolution of Saxo-Thuringia at the margin of Gondwana in the light of single zircon geochronology and basin development (central European Variscides, Germany). In: Franke, W., Haak, V., Oncken, O., Tanner, D. (Eds.), Orogenic Processes: Quantification and Modelling in the Variscan Belt, Geological Society of London Special Publication, vol. 179, pp. 131–153. https://doi.org/10.1144/GSL.SP.2000.179.01.10.

Linnemann, U., Gerdes, A., Drost, K., Buschmann, B., 2007. The continuum between Cadomian orogenesis and opening of the Rheic Ocean: constraints from LA-ICP-MS U-Pb zircon dating and analysis of platetectonic setting (Saxo-Thuringian zone, northeastern Bohemian Massif, Germany). In: Linnemann, U., Nance, D., Kraft, P., Zulauf, G. (Eds.), The Evolution of the Rheic Ocean: From Avalonian-Cadomian Active Margin to Alleghenian-Variscan Collision, Geological Society of America Special Paper, vol. 423, pp. 61–96.

Linnemann, U., Pereira, F., Jeffries, T.E., Drost, K., Gerdes, A., 2008. The Cadomian orogeny and the opening of the Rheic Ocean: the diacrony of geotectonic processes constrained by LA-ICP-MS U-Pb zircon dating (Ossa-Morena and Saxo-Thuringian zones, Iberian and Bohemian Massifs). Tectonophysics 461, 21–43.

Ludwig, K.R., 2001. SQUID 1.02, a User's Manual. Berkeley Geochronology Center Special Publication No. 2, 2455 Ridge Road, Berkeley, CA 94709, US.

Ludwig, K.R., 2003. Isoplot/Ex Version 3.0: a Geochronological Toolkit for Microsoft Excel, 4. Berkeley Geochronology Center, Special Publication, p. 70.

Maino, M., Seno, S., 2016. The thrust zone of the Ligurian Penninic basal contact (Monte Fronté, Ligurian Alps, Italy). Journal of Maps 12 (1), 341–351. https://doi.org/10.1080/17445647.2016.1213669.

Maino, M., Dallagiovanna, G., Dobson, K., Gaggero, L., Persano, C., Seno, S., Stuart, F.M., 2012a. Testing models of orogen exhumation using zircon (U–Th)/He thermochronology: insights from the Ligurian Alps, Northern Italy. Tectonophysics 560/561, 84–93. https://doi.org/10.1016/j.tecto.2012.06.045.

Maino, M., Dallagiovanna, G., Gaggero, L., Seno, S., Tiepolo, M., 2012b. U–Pb zircon geochronological and petrographic constraints on late to post-collisional Variscan magmatism and metamorphism in the Ligurian Alps, Italy. Geological Journal 47 (6), 632–652. https://doi.org/10.1002/gj.2421.

Maino, M., Decarlis, A., Felletti, F., Seno, S., 2013. Tectono-sedimentary evolution of the Tertiary Piedmont Basin (NW Italy) within the Oligo–Miocene central Mediterranean geodynamics. Tectonics 32, 593–619. https://doi.org/10.1002/tect.20047.

Maino, M., Bonini, L., Dallagiovanna, G., Seno, S., 2015a. Large sheath folds in the Briançonnais of the Ligurian Alps reconstructed by analysis of minor structures and stratigraphic mapping. Journal of Maps 11 (1), 157–167. https://doi.org/10.1080/17445647.2014.959568.

Maino, M., Casini, L., Ceriani, A., Decarlis, A., Di Giulio, A., Seno, S., Setti, M., Stuart, F.M., 2015b. Dating shallow thrusts with zircon (U-Th)/He thermochronometry – the shear heating connection. Geology 43 (6), 495–498. https://doi.org/10.1130/G36492.1.

Martini, P., Tongiorgi, M., Oggiano, G., Cocozza, T., 1991. Alluvial fan to marine shelf transition in SW Sardinia, Western Mediterranean Sea: tectonically ("Sardic Phase") influenced clastic Ordovician sedimentation. Sedimentary Geology 72, 97–115.

Matte, P., 1986. Tectonics and plate tectonics model for the Variscan belt of Europe. Tectonophysics 126, 329–374.

Matte, P., 2001. The Variscan collage and orogeny (480-290 Ma) and the tectonic definition of the Armorica microplate: a review. Terra Nova 13, 122–128.

Ménot, R.-P., Peucat, J.J., Scarenzi, D., Piboule, M., 1988. 496 My age of plagiogranites in the Chamrousse ophiolite complex (External Crystalline Massifs in the French Alps): evidence of a Lower Palaeozoic oceanization. Earth and Planetary Science Letters 88, 82–92.

Messiga, B., Oxilia, M., Piccardo, G.B., Vanossi, M., 1981. Fasi metamorfiche e deformazioni Alpine nel Brianzonese e nel Pre-Piemontese – Piemontese esterno delle Alpi Liguri: un possible modello evolutivo. Rendiconti della Società Italiana di Mineralogia e Petrologia 38 (1), 261–280 (in French).

Messiga, B., Tribuzio, R., Scambelluri, M., 1992. Mafic eclogites from the valosio crystalline massif (Ligurian Alps, Italy). Schweizerische Mineralogische Und Petrographische Mitteilungen 72, 365–377.

Micheletti, F., Barbey, P., Fornelli, A., Piccarreta, G., Deloule, E., 2007. Latest Precambrian to Early Cambrian U–Pb zircon ages of augen gneisses from Calabria (Italy), with inference to the Alboran microplate in the evolution of the peri-Gondwana terranes. International Journal of Earth Sciences 96 (5), 843–860.

Micheletti, F., Fornelli, A., Piccarreta, G., Tiepolo, M., 2011. U–Pb zircon data of Variscan meta-igneous and igneous acidic rocks from an Alpine shear zone in Calabria (southern Italy). International Journal of Earth Sciences 100 (1), 139–155.

Molina, M., 2002. Analisi petrologica e geocronologica di litotipi del basamento e del tegumento delle Alpi Liguri e del basamento della Sardegna nordorientale (PhD thesis). University of Genoa (in Italian with English abstract).

Montero, C., Bea, F., González-Lodeiro, F., Talavera, C., Whitehouse, M.J., 2007. Zircon ages of the metavolcanic rocks and metagranites of the Ollo de Sapo domain in central Spain: implications for the Neoproterozoic to early Palaeozoic evolution

of Iberia. Geological Magazine 144, 963–976. https://doi.org/10.1017/S0016756807003858.
Müller, B., Klötzli, U., Schaltegger, U., Flisch, M., 1996. Early Cambrian oceanic plagiogranite in the Silvretta nappe, eastern Alps: geochemical, zircon U-Pb and Rb-Sr data from garnet-hornblende-plagioclase gneisses. Geologische Rundschau 85, 822–831. https://doi.org/10.1007/BF02440113.
Nance, R.D., Gutiérrez-Alonso, G., Keppie, J.D., Linnemann, U., Murphy, J.B., Quesada, C., Strachan, R.A., Woodcock, N.H., 2010. Evolution of the Rheic Ocean. Gondwana Research 17 (2–3), 194–222.
Navidad, M., Castiñeiras, P., Casas, J.M., Liesa, M., Fernández Suárez, J., Barnolas, A., Carreras, J., Gil-Peña, I., 2010. Geochemical characterization and isotopic age of Caradocian magmatism in the northeastern Iberian Peninsula: insights into the Late Ordovician evolution of the northern Gondwana margin. Gondwana Research 17, 325–337. https://doi.org/10.1016/j.gr.2009.11.013.
Navidad, M., Castiñeiras, P., 2011. Early Ordovician magmatism in the northern Central Iberian zone (Iberian Massif): new U-Pb (SHRIMP) ages and isotopic Sr-Nd data. In: Gutiérrez-Marco, J.C., Rábano, I., García-Bellido, D. (Eds.), The Ordovician of the World, vol. 14. Instituto Geológico y Minero de España, Cuadernos del Museo Geominero, Madrid, pp. 391–398.
Oggiano, G., Gaggero, L., Funedda, A., Buzzi, L., Tiepolo, M., 2010. Multiple early Palaeozoic volcanic events at the northern Gondwana margin: U-Pb age evidence from the southern Variscan branch (Sardinia, Italy). Gondwana Research 17, 44–58. https://doi.org/10.1016/j.gr.2009.06.001.
Paces, J.B., Miller, J.D., 1993. Precise U–Pb ages of Duluth Complex and related mafic intrusions, Northern Minnesota: geochronological insight to physical, petrogenic, and tectonomagmatic processes associated with the 1.1 Ga midcontinent rift system. Journal of Geophysical Research 98 (B8), 13997–14013.
Paquette, L., Ménot, R.P., Peucat, J.J., 1989. REE, Sm-Nd and U-Pb zircon study of eclogites from the Alpine External massifs (western Alps): evidence for crustal contamination. Earth and Planetary Science Letters 96, 181–198. https://doi.org/10.1016/0012-821X(89)90131-3.
Poller, U., Liebetrau, V., Todt, W., 1997. U–Pb single-zircon dating under cathodoluminescence control (CLC-method): application to polymetamorphic orthogneisses. Chemical Geology 139, 287–297.
Rode, S., Rösel, D., Schulz, B., 2012. Constraints on the Variscan P-T evolution by EMP Th-U-Pb monazite dating in the polymetamorphic Austroalpine Oetztal-Stubai basement (eastern Alps). Zeitschrift der Deutschen Gesellschaft für Geowissenschaften 163, 43–67. https://doi.org/10.1127/1860-1804/2012/0163-0043.
Roger, F., Respaut, J.P., Brunel, M., Matte, Ph, Paquette, J.L., 2004. Première datation U-Pb des orthogneiss oeillés de la zone axiale de la Montgane Noire (Sud du Massif central): Nouveaux témoins du magmatisme ordovicien dans la chaîne varisque. Comptes Rendus de l'Académie des Sciences, Geoscience 336, 19–28 (in Italian). https://doi.org/10.1016/j.crte.2003.10.014.
Rossi, P., Oggiano, G., Cocherie, A., 2009. A restored section of the 'southern Variscan Realm' across the Corsica–Sardinia microcontinent. Comptes Rendus Geoscience 341, 224–238.
Rubatto, D., 2002. Zircon trace element geochemistry: partitioning with garnet and the link between U–Pb ages and metamorphism. Chemical Geology 184 (1), 123–138. https://doi.org/10.1016/S0009-2541(01)00355-2.
Rubatto, D., Schaltegger, U., Lombardo, B., Colombo, F., Compagnoni, R., 2001. Complex Palaeozoic magmatic and metamorphic evolution in the Argentera Massif (Western Alps) resolved with U–Pb dating. Swiss Bulletin of Mineralogy and Petrology 81, 213–228.
Rubio-Ordóñez, A., Valverde-Vaquero, P., Corretgé, L.G., Cuesta-Fernández, A., Gallastegui, G., Fernández-González, M., Gerdes, A., 2012. An Early Ordovician tonalitic–granodioritic belt along the Schistose-Greywacke domain of the Central Iberian zone (Iberian Massif, Variscan belt). Geological Magazine 149 (5), 927–939. https://doi.org/10.1017/S0016756811001129.
Sánchez Martínez, S., Gerdes, A., Arenas, R., Abati, J., 2012. The bazar ophiolite of NW Iberia: a relic of the Iapetus–Tornquist ocean in the variscan suture. Terra Nova 24, 283–294. https://doi.org/10.1111/j.1365-3121.2012.01061.x.
Schaltegger, U., 1993. The evolution of the polymetamorphic basement in the central Alps unraveled by precise U-Pb zircon dating. Contributions to Mineralogy and Petrology 113, 466–478. https://doi.org/10.1007/BF00698316.
Schaltegger, U., Gebauer, D., 1999. Pre-Alpine geochronology of the Central, Western and Southern Alps. Schweizerische Mineralogische und Petrographische Mitteilungen 79, 79–87.
Schaltegger, U., Gebauer, D., von Quadt, A., 2002. The mafic-ultramafic rock association of Loderio-Biasca (lower Pennine nappes, Ticino, Switzerland): Cambrian oceanic magmatism and its bearing on early Palaeozoic paleogeography. Chemical Geology 186, 265–279. https://doi.org/10.1016/S0009-2541(02)00005-0.
Schaltegger, U., Abrecht, J., Corfu, F., 2003. The Ordovician orogeny in the Alpine basement: constraints from geochronology and geochemistry in the Aar Massif (central Alps). Schweizerische Mineralogische und Petrographische Mitteilungen 83, 183–195.
Schmid, S., Pfiffner, A., Froitzheim, N., Schönborn, G., Kissling, E., 1996. Geophysical-geological transect and tectonic evolution of the Swiss–Italian Alps. Tectonics 15, 1036–1064. https://doi.org/10.1029/96TC00433.
Schulz, B., Steenken, A., Siegesmund, S., 2008. Geodynamic evolution of an Alpine terrane—the Austroalpine basement to the south of the Tauern Window as a part of the Adriatic plate (eastern Alps). In: Siegesmund, S., Fügenschuh, B., Froitzheim, N. (Eds.), Tectonic Aspects of the Alpine-Dinaride-Carpathian System: Geological Society of London Special Publication 298, pp. 5–44.
Schulz, B., von Raumer, J., 2011. Discovery of Ordovician–Silurian metamorphic monazite in garnet metapelites of the Alpine External Aiguilles Rouges Massif. Swiss Journal of Geosciences 104.1, 67–79. https://doi.org/10.1007/s00015-010-0048-7.
Seno, S., Dallagiovanna, G., Vanossi, M., 2005. A kinematic evolutionary model for the Penninic sector of the central Ligurian Alps. International Journal of Earth Sciences 94, 114–129.
Seno, S., Dallagiovanna, G., Gaggero, L., Felletti, F., Pellegrini, L., 2010. Cairo Montenotte – 228 Sheet, Geological Map of Italy, 1:50.000 Scale. ISPRA, Rome, Italy. Available online at: http://www.isprambiente.gov.it/Media/carg/liguria.html.
Spencer, C.J., Kirkland, C.L., Taylor, R.J.M., 2016. Strategies towards statistically robust interpretations of in situ U–Pb zircon geochronology. Geoscience Frontiers 7 (4), 581–589. https://doi.org/10.1016/j.gsf.2015.11.006.
Stampfli, G.M., von Raumer, J., Wilhem, C., 2011. The distribution of Gondwana derived terranes in the early Palaeozoic. In: The Ordovician of the World, vol. 14. Instituto Geológico y Minero de España, Cuadernos del Museo Geominero, Madrid, pp. 567–574.
Tera, F., Wasserburg, G.J., 1972. U-Th-Pb systematics in three Apollo 14 basalts and the problem of initial Pb in lunar rocks. Earth and Planetary Science Letters 14 (3), 281–304.
Thöny, W.F., Tropper, P., Schennach, F., Krenn, E., Finger, F., Kaindl, R., Bernhard, F., Hoinkes, G., 2008. The metamorphic evolution of migmatites from the Ötztal complex (Tyrol, Austria) and constraints on the timing of the pre-Variscan high-T event in the eastern Alps. Swiss Journal of Geosciences 101 (Suppl. 1), 111–126. https://doi.org/10.1007/s00015-008-1290-0.
Tiepolo, M., 2003. In situ Pb geochronology of zircon with laser ablation inductively coupled plasma sector field mass spectrometry. Chemical Geology 192, 1–19.
Trombetta, A., Cirrincione, R., Corfu, F., Mazzoleni, P., Pezzino, A., 2004. Mid-Ordovician U–Pb ages of porphyroids in the Peloritan Mountains (NE Sicily): palaeogeographical implications for the evolution of the Alboran microplate. Journal of the Geological Society 161 (2), 265–276.
Valverde-Vaquero, P., Dunning, G.R., 2000. New U-Pb ages for Early Ordovician magmatism in central Spain. Journal of the Geological Society of London 157, 15–26. https://doi.org/10.1144/jgs.157.1.15.
van Achterberg, E., Ryan, C.G., Jackson, S.E., Griffin, W., 2001. Data reduction software for LA–ICP–MS. In: Sylvester, P. (Ed.), Laser Ablation ICPMS in the Earth Science: Principles and Applications, vol. 29. Mineralogical Association of Canada, pp. 239–243.
Vanossi, M., Cortesogno, L., Galbiati, B., Messiga, B., Piccardo, G.B., Vannucci, R., 1986. Geologia delle Alpi Liguri: dati, problemi, ipotesi. Memorie della Società Geologica Italiana 28, 5–75.
von Raumer, J.F., 1998. The Palaeozoic evolution in the Alps – from Gondwana to Pangea. Geologische Rundschau 87, 407–435. https://doi.org/10.1007/s005310050219.
von Raumer, J.F., Stampfli, G.M., 2008. The birth of the Rheic Ocean – Early Palaeozoic subsidence patterns and tectonic plate scenarios. Tectonophysics 461, 9–20. https://doi.org/10.1016/j.tecto.2008.04.012.
von Raumer, J.F., Stampfli, G.M., Borel, G., Bussy, F., 2002. The organization of pre-Variscan basement areas at the north-Gondwanan margin. International Journal of Earth Sciences 91, 35–52. https://doi.org/10.1007/s005310100200.
von Raumer, J.F., Stampfli, G.A., Bussy, F., 2003. Gondwana-derived microcontinents-the constituents of the Variscan and Alpine collisional orogens. Tectonophysics 365 (1–4), 7–22.
von Raumer, J., Bussy, F., Stampfli, G., 2009. The Variscan evolution in the Alps—and place in their Variscan framework. Comptes Rendus de l'Académie des Sciences, Geosciences 341, 239–252.
von Raumer, J.F., Bussy, F., Schaltegger, U., Schulz, B., Stampfli, G.M., 2013. Pre-Mesozoic Alpine basements. Their place in the European Palaeozoic framework. The Geological Society of America Bulletin 125 (1e2), 89–108.
Wiedenbeck, M., Alle, P., Corfu, F., Griffin, W.L., Meier, M., Oberli, F., Vonquadt, A., Roddick, J.C., Speigel, W., 1995. Three natural zircon standards for U-Th-Pb, Lu-Hf, trace element and REE analyses. Geostandards Newsletter 19, 1–23.
Williams, I.S., 1998. U–Th–Pb geochronology by ion microprobe. Reviews in Economic Geology 7, 1–35.
Williams, I.S., Fiannacca, P., Cirrincione, R., Pezzino, A., 2012. Peri-Gondwanan origin and early geodynamic history of NE Sicily: a zircon tale from the basement of the Peloritani Mountains. Gondwana Research 22 (3), 855–865.
Winchester, J.A., Patočka, F., Kachlik, V., Melzer, M., Nawakowski, C., Crowley, Q.G., Floyd, P.A., 2003. Geochemical discrimination of metasedimentary sequences in the Krkonose-Jisera terrane (West Sudetes, Bohemian Massif). Geologica Carpathica 54, 267–280.
Ziegler, P., 1984. Caledonian and Hercynian crustal consolidation of western and central Europe – a working hypothesis. Geologie en Mijnbouw 63, 93–108.